こっている現象を，よりヒトに近い動物を用いて慎重に検証していくことが必要かもしれない。加えて，臨床応用には安全性を確保することが絶対条件であることからもマウスよりも長期間モニターできる動物を用いた移植試験などが重要になってくることであろう。

●文 献

1) Gadue P, Huber TL, Paddison PJ et al : *Proc Natl Acad Sci U S A* 103 : 16806-16811, 2006
2) McDowell RK, Gazelle GS, Murphy BL, et al : *J Comput Assist Tomogr* 21 : 383-388, 1997
3) Sumi T, Tsuneyoshi N, Nakatsuji N et al : *Development* 135 : 2969-2979, 2008
4) Liu P, Wakamiya M, Shea MJ et al : *Nat Genet* 22 : 361-365, 1999
5) D'Amour KA, Agulnick AD, Eliazer S et al : *Nature Biotechnol* 23 : 1534-1541, 2005
6) McLean AB, D'Amour KA, Jones KL, et al : *Stem Cells* 25 : 29-38, 2007
7) Hebrok M, Kim SK, St Jacques B et al : *Development* 127 : 4905-4913, 2000
8) Maldonado TS, Kadison AS, Crisera CA et al : *J Gastrointest Surg* 4 : 269-275, 2000
9) Hardikar AA, Marcus-Samuels B, Geras-RaakaE et al : *Proc Natl Acad Sci U S A* 100 : 7117-7122, 2003
10) Jung SE, Kim DY, Park KW et al : *World J Surg* 23 : 233-236, 1999
11) D'Amour KA, Bang AG, Eliazer S et al : *Nat Biotechnol* 24 : 1392-1401, 2006
12) Rezania A, Bruin JE, Riedel MJ et al : *Diabetes* 61 : 2016-2029, 2012
13) Schulz TC, Young HY, Agulnick AD et al : *PLoS One* 7 : e37004, 2012
14) Chung WS, Shin CH, Stainier DY : *Dev Cell* 15 : 738-748, 2008
15) Tremblay KD, Zaret KS : *Dev Biol* 280 : 87-99, 2005
16) Deutsch G, Jung J, Zheng M et al : *Development* 128 : 871-881, 2001
17) Spence JR, Lange AW, Lin SC et al : *Dev Cell* 17 : 62-74, 2009
18) Ahlgren U, Jonsson J, Jonsson L et al : *Genes Dev* 12 : 1763-1768, 1998
19) Gradwohl G, Dierich A, LeMeur M et al : *Proc Natl Acad Sci U S A* 97 : 1607-1611, 2000
20) Gu G, Dubauskaite J, Melton DA : *Development* 129 : 2447-2457, 2002
21) Jensen J, Heller RS, Funder-Nielsen T et al : *Diabetes* 49 : 163-176, 2000
22) Kawaguchi Y, Cooper B, Gannon M et al : *Nat Genet* 32 : 128-134, 2002
23) Fukuda A, Kawaguchi Y, Furuyama K et al : *J Clin Invest* 116 : 1484-1493, 2006
24) Bhushan A, Itoh N, Kato S et al : *Development* 128 : 5109-5117, 2001
25) Hart A, Papadopoulou S, Edlund H : *Dev Dyn* 228 : 185-193, 2003
26) Norgaard GA, Jensen JN, Jensen J : *Dev Biol* 264 : 323-338, 2003
27) Kim SK, MacDonald RJ : *Curr Opin Genet Dev* 12 : 540-547, 2002
28) Wilson ME, Kalamaras JA, German MS : *Mech Dev* 115 : 171-176, 2002
29) Johansson KA, Dursun U, Jordan N et al : *Dev Cell* 12 : 457-465, 2007
30) Schwitzgebel VM, Scheel DW, Conners JR et al : *Development* 127 : 3533-3542, 2000
31) Finegood DT, Scaglia L, Bonner-Weir S : *Diabetes* 44 : 249-256, 1995
32) Sander M, Sussel L, Conners J et al : *Development* 127 : 5533-5540, 2000
33) Böhm M, Zmijewski MA, Wasiewicz T et al : *Exp Dermatol* 21 : 541-543, 2012
34) Borowiak M, Melton DA : *Curr Opin Cell Biol* 21 : 727-732, 2009
35) Chen S, Borowiak M, Fox JL et al : *Nat Chem Biol* 5 : 258-265, 2009
36) Kunisada Y, Tsubooka-Yamazoe N, Shoji M et al : *Stem Cell Res* 8 : 274-284, 2012
37) Saisho Y, Harris PE, Butler AE et al : *J Mol Histol* 39 : 543-551, 2008
38) Sakano D, Shiraki N, Kikawa K et al : *Nat Chem Biol* 10 : 141-148, 2014
39) Maehr R, Chen S, Snitow M et al : *Proc Natl Acad Sci U S A* 106 : 15768-15773, 2009
40) Ohmine S, Squillace KA, Hartjes KA et al : *Aging (Albany NY)* 4 : 60-73, 2012
41) Hanna J, Wernig M, Markoulaki S et al : *Science* 318 : 1920-1923, 2007

メチオニンの代謝はヒトのES細胞およびiPS細胞の未分化な状態の維持および分化を制御している

白木伸明・粂 昭苑

(熊本大学発生医学研究所 多能性幹細胞分野)

email:粂 昭苑

Methionine metabolism regulates maintenance and differentiation of human pluripotent stem cells.
Nobuaki Shiraki, Yasuko Shiraki, Tomonori Tsuyama, Fumiaki Obata, Masayuki Miura, Genta Nagae, Hiroyuki Aburatani, Kazuhiko Kume, Fumio Endo, Shoen Kume
Cell Metabolism, 19, 780-794 (2014) http://www.ncbi.nlm.nih.gov/pubmed/24746804

目 次

要 約

マウスのES細胞およびiPS細胞においてはスレオニンの代謝がさかんであり，スレオニンを除去した培地では生育できないことがわかっていたが，ヒトのES細胞およびiPS細胞におけるアミノ酸の代謝に関しては報告がなかった．筆者らは，遺伝子発現の解析および代謝産物の定量により，ヒトのES細胞およびiPS細胞においてはメチオニンの代謝が非常にさかんであることを見い出した．ヒトのES細胞およびiPS細胞をメチオニン除去培地で5時間培養すると，メチオニンの代謝産物であり生体におけるさまざまなメチル化反応において利用されている*S*-アデノシルメチオニンの濃度が顕著に低下し，p53シグナルの活性化，NANOGの発現の低下がひき起こされた．未分化な状態を維持する過程においてメチオニン除去培地で短時間培養することにより，細胞の増殖は抑制され，のちの三胚葉への分化は促進された．さらに，未分化な細胞と比べ分化した内胚葉細胞はメチオニンの要求性が低いという性質を利用して，分化を誘導する過程においてメチオニン除去培地を用いることにより未分化な細胞を選択的に除去することに成功した．この研究では，これまで不明であったヒトのES細胞およびiPS細胞における未分化な状態の維持および分化の機構におけるメチオニン代謝の重要性を明らかにし，*S*-アデノシルメチオニンがその制御にはたらくことをはじめて報告した．

はじめに

これまで，筆者らの研究室では，ES細胞（embryonic stem cell，胚性幹細胞）およびiPS細胞（induced pluripotent stem cell，人工多能性幹細胞）を用いて内胚葉の発生および分化の機構を解明してきた．その過程で，細胞外マトリックスや低分子化合物を利用して細胞外の環境を変化させることにより，ES細胞およびiPS細胞から肝臓[1]，膵臓[2,3]，小腸細胞[4]への選択的な分化を誘導することにも成功した．ES細胞およびiPS細胞といった多能性をもつ幹細胞は，分化した細胞とは異なる代謝プログラムを保持していることがわかっており，その代謝プログラムが幹細胞における未分化な状態の維持や自己複製能などに関与することが明らかになってきている[5-7]．ES細胞およびiPS細胞におけるアミノ酸代謝については，マウスのES細胞の生存にはスレオニンが必須であることが明らかにされており，未分化なES細胞ではスレオニンからグリシンおよびアセチルCoAを合成する際の律速酵素であるスレオニン脱水素酵素が高く発現していることがわかっていた[8]．また，マウスのES細胞およびiPS細胞においては，スレオニンから複数のステップをへて合成される*S*-アデノシルメチオニンがエピゲノムの状態を維持するために重要であることも報告されていた[9]．しかし，ヒトのES細胞およびiPS細胞においてはこのスレオニン脱水素酵素は発現していないことがわかっており，ヒトのES細胞およびiPS細胞におけるアミノ酸代謝の役割は不明であった．この研究では，ヒトのES細胞およびiPS細胞は未分化な状態では高いメチオニン要求性を示し，このメチオニン要求性は分化にともない減少することを見い出した．

1．メチオニンの除去によりヒトのES細胞およびiPS細胞は細胞周期が停止し細胞死が起こる

未分化なヒトのES細胞およびiPS細胞におけるアミノ酸の要求性について，2つのヒトES細胞株および2つのヒトiPS細胞株を用いて検討した．9種類の必須アミノ酸をそれぞれ1つずつ除去した未分化維持培地を調製し，それぞれの培地で48時間培養したのち細胞数を評価した．ロイシン，リジン，トリプトファン，メチオニンの除去により細胞数の減少が確認でき，なかでも，メチオニンの除去による減少がもっとも大きく，完全培地で培養した場合の5％以下にまで細胞数は顕著に減少した．さらに，メチオニンの要求性について評価したところ，未分化なヒトのES細胞およびiPS細胞の良好な生育には25 μM以上のメチオニンが必要であることがわかった（完全培地は，約120 μMのメチオニンを含む）．つづいて，メチオニンを除去したのちの細胞死，細胞の増殖，細胞周期について継時的に評価した．その結果，未分化なヒトのES細胞およびiPS細胞はメチオニンの除去から5時間後には顕著な増殖の抑制を示し，24時間後にはG0期あるいはG1期において細胞周期が停止しアポトーシスの起こることがわかった．

2．S-アデノシルメチオニンはヒトのES細胞およびiPS細胞の生存において重要である

ヒトのES細胞およびiPS細胞の生存にはメチオニンが非常に重要であることがわかったことから，メチオニンの代謝の変化について遺伝子発現の解析および代謝産物の定量により評価した（図1）．遺伝子発現はマイクロアレイ法により解析し，代謝産物については細胞内のメチオニン，*S*-アデノシルメチオニン，*S*-メチル-5'-チオアデノシン，*S*-アデノシルホモシステイン，および，培養液中のホモシステインをUPLC-MS/MS法により定量した．その結果，メチオニンの除去から5時間後には*DNMT3B*遺伝子および*MAT2B*遺伝子の顕著な発現の低下が確認され，細胞内のメチオニン，*S*-メチル-5'-チオアデノシン，*S*-アデノシルメチオニンの濃度が顕著に低下した．興味深いことに，完全培地での培養では確認できるホモシステインの細胞外への排出が，メチオニン除去培地での培養ではまったく起こらなくなった．さらに，*S*-アデノシルメチオニンからメチオニンへのサルベージ回路の中間代謝産物である*S*-メチル-5'-チオアデノシンを添加することにより，メチオニンの除去により停止したホモシステインの細胞外への排出が完全に回復することも確認された．以上のことから，ヒトのES細胞およびiPS細胞はメチオニン除去培地での培養を開始すると，すみやかにメチオニン代謝回路が停止することが明らかになった．また，ヒトのES細胞およびiPS細胞においてメチオニンへのサルベージ回路がはたらいていることも確認された．

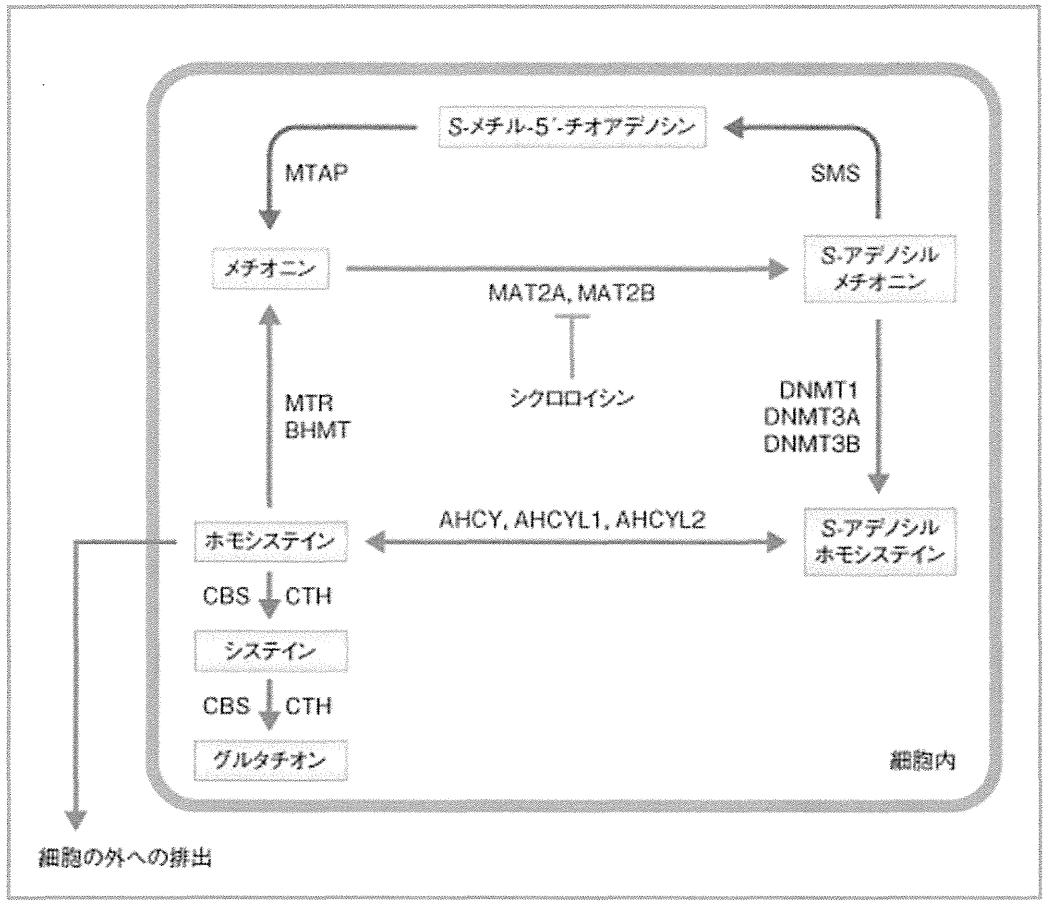

図1　メチオニン代謝回路

青色の線は*S*-アデノシルメチオニンからメチオニンへのサルベージ回路を示す.

[Download] http://first.lifesciencedb.jp/wp-content/uploads/2014/05/Kume-Cell-Metabolism-14.5.2-Fig.1.jpg

メチオニン代謝回路において, メチオニンあるいはその代謝産物である*S*-アデノシルメチオニンのどちらがヒトのES細胞およびiPS細胞の生存により重要な役割をはたしているのかについて評価した. *S*-アデノシルメチオニンはメチオニンを除去したのちの細胞死を抑制したが, メチオニンへのサルベージ回路における律速酵素であるSMSをノックダウンした場合にも*S*-アデノシルメチオニンの添加により細胞死が抑制された. このことは, *S*-アデノシルメチオニンがサルベージ回路によりメチオニンとなってはたらいているのではなく, *S*-アデノシルメチオニンそれ自体が細胞死に関与していることを意味した. さらに, MAT2AおよびMAT2Bの阻害剤であるシクロロイシンはメチオニンの除去と同様にヒトのES細胞およびiPS細胞に細胞死を誘導したが, シクロロイシンの添加から5時間後の細胞内の*S*-アデノシルメチオニンの濃度は対照の半分にまで低下した一方, メチオニンの濃度は対照の2倍に増加することが確認された. この結果からも, 細胞内における*S*-アデノシルメチオニンの低下が細胞死をひき起こすことが示唆された. 以上の結果から, ヒトのES細胞およびiPS細胞の生存にはメチオニン代謝回路, とりわけ, 細胞内の*S*-アデノシルメチオニンが重要な役割をはたしていることがわかった.

3. メチオニンの除去によりp53シグナルが活性化される

メチオニンを除去したのちにはメチオニンの代謝が停止し*S*-アデノシルメチオニンの濃度が低下したことから, ほかのシグナル分子の変化についても, マイクロアレイ解析, ウェスタンブロット解析, および, 免疫細胞化学的な解析により評価した. その結果, メチオニンの除去から5時間後にはすでに細胞周期および細胞死に関連する多くの遺伝子の発現が上昇していることがわかった. 細胞死に関与する重要なシグナル分子であるp53に関しては, mRNAの量に変化はなかったがタンパク質の量が顕著に増加し, その増加は*S*-アデノシルメチオニンの添加により阻害されることが確認された. さらに, このp53の発現の上昇は培地のメチオニン濃度が6 μ M以下の場合に起こり, ほかのアミノ酸の除去では起こらないことも確認された. メチオニンを除去したのちの細胞死にp53の関与することが示唆されたため, p53をノックダウンした細胞においてメチオニンを除去したところ細胞死が抑制された. 以上の結果から, ヒトのES

細胞およびiPS細胞をメチオニン除去培地で培養するとp53のタンパク質レベルの発現が上昇し，その結果として，細胞周期の停止および細胞死の起こることがわかった．

4. 未分化な状態におけるメチオニンの除去によりのちの分化は促進される

メチオニンを除去したのちに起こる細胞内の*S*-アデノシルメチオニンの低下がヒストンメチル化およびDNAメチル化にあたえる影響について検討した．マウスのES細胞においても，スレオニンの除去により結果的に*S*-アデノシルメチオニンの減少の起こることが報告されており，その際に，ヒストンH3の4番目のLysのトリメチル化の低下することがわかっていた．そこで，ヒストンH3における各種のメチル化への影響をウェスタンブロット法により評価したところ，メチオニンの除去あるいはシクロロイシンの処理から5時間後に，ヒストンH3の4番目のLysのトリメチル化の顕著に低下することが確認された．一方，ヒストンH3の9番目のLysのトリメチル化，27番目のLysのトリメチル化，36番目のLysのトリメチル化については，メチオニンの除去から24時間後においても変化は確認されなかった．このおのおののLysメチル化に対するメチオニン除去の効果の違いの原因については不明であり，さらなる検討が必要である．さらに，DNAメチル化に対する影響についてマイクロアレイ法を用いて網羅的に評価した．解析の結果，メチオニンの除去から5時間後には広い範囲でDNAメチル化の低下がみられたが，特定の遺伝子にかたよるものではなく，その低下の程度も遺伝子の発現に影響をあたえるほど強いものではなかった．

ヒトのES細胞およびiPS細胞はメチオニン除去培地で培養すると一時的に増殖の停止することがわかったので，その状態における未分化マーカーの発現について調べた．その結果，メチオニンの除去から5時間後にNANOGのmRNAレベルおよびタンパク質レベルでの発現の低下が確認された．ほかの未分化マーカーであるOct3/4については発現に変化はみられなかった．このNANOGの発現低下は*S*-アデノシルメチオニンの添加により抑制され，さらに，ほかのアミノ酸の除去では起こらないこともわかった．メチオニンの短時間の除去ののちの増殖の停止に関しては，のちに完全培地に置き換えることにより回復が可能であることがわかっていたため，この短時間のメチオニン除去ののちのNANOGの発現低下を分化の促進に利用できるのではないかと考えた．そこで，ヒトiPS細胞株を未分化な状態においてメチオニン除去培地で10時間培養したのち，内胚葉，中胚葉，外胚葉への分化培地にそれぞれ置換して分化の誘導効率を評価した．その結果，それぞれの胚葉への分化の効率は約3倍も上昇した．内胚葉への分化の促進効果については，ほかのヒトiPS細胞株およびヒトES細胞株においても確認した．以上のことから，ヒトのES細胞およびiPS細胞においては，メチオニンの代謝阻害によりヒストンH3の4番目のLysのトリメチル化の低下およびNANOGの発現の低下がひき起こされ，のちの胚葉への分化の起こりやすい状態へと移行していることがわかった．

5. 分化の過程におけるメチオニンの除去により未分化な細胞において選択的に細胞死が誘導される

未分化な細胞および分化した細胞におけるメチオニン代謝の違いについて，遺伝子発現の解析および代謝産物の定量により比較した．分化した細胞としては，ヒトES細胞株から分化を誘導した内胚葉を用いた．遺伝子発現の解析の結果，*MAT*遺伝子や*DNMT*遺伝子といったメチオニン代謝にかかわる酵素をコードする遺伝子の多くが未分化な細胞において高く発現していた．また，培地中のメチオニン濃度を経時的に定量した結果，未分化な細胞は分化した細胞に比べ単位時間あたり約5倍のメチオニンを消費していることもわかった．さらに，細胞外へのホモシステインの排出について評価した結果，分化した細胞では未分化な細胞の約半分であった．さきに述べたように，未分化な細胞はメチオニン除去培地で培養するとホモシステインの細胞外への排出が停止するが，分化した細胞ではホモシステインの排出量に変化はなかった．以上のことから，未分化な細胞は分化した細胞に比べメチオニン代謝が非常にさかんであり，その生育により多くのメチオニンが必要であることがわかった．

ヒトのES細胞およびiPS細胞は細胞株のあいだで分化能に差のあることがよく知られている[10]．そこで，すでに構築されている支持細胞を用いた分化の誘導系を用いて，細胞株のあいだの分化能の違いについて評価した．その結果，同じ培養条件で内胚葉へ分化させた場合に，ヒトES細胞株khES3およびヒトiPS細胞株253G1株は非常によく分化したものの，ヒトES細胞株khES1およびヒトiPS細胞株201B7株は10日間にわたり分化を誘導しても未分化な細胞の残存することがわかった．未分化な細胞と分化した内胚葉細胞にはメチオニンの要求性に違いのあることがわかって

いたため，分化の途中からメチオニン除去培地で培養することにより未分化な細胞のみを選択的に除去できるのではないかと考えた．ヒトES細胞株khES1およびヒトiPS細胞株201B7株を用いて培養8日目から10日目までの2日間にわたりメチオニン除去培地で培養した結果，内胚葉に影響をあたえることなく未分化な細胞に対し選択的に細胞死が誘導され，相対的に内胚葉への分化の効率が上昇することがわかった．ヒトiPS細胞株201B7株について，のちに肝臓への分化を誘導したところ，最終的なアルブミンの発現量および分泌量が約3倍にも増加することがわかった．このことから，分化の過程においてメチオニン除去培地で培養することにより残存する未分化な細胞を除去することが可能であり，分化の効率の悪い細胞株を利用する場合は非常に有効な手段となりうることがわかった．

おわりに

今回の研究において，ヒトのES細胞およびiPS細胞の生存にはメチオニンが必須であり，その代謝産物である*S*-アデノシルメチオニンを介してヒトのES細胞およびiPS細胞の未分化な状態の維持および分化が制御されていることを見い出した(図2)．マウスの場合は*S*-アデノシルメチオニンの供給源としてスレオニンが積極的に利用されているが，ヒトの場合はメチオニンがおもに利用されていることが明らかになった．さらに，ヒトのES細胞およびiPS細胞のもつメチオニン代謝の特性を分化の誘導に応用した結果，未分化な状態においてメチオニンを除去したのち，内胚葉，中胚葉，外胚葉へとそれぞれ分化を誘導すると，顕著な分化の促進効果がみられることを確認した．さらに，内胚葉への分化の誘導の過程においてメチオニン除去培地で培養することにより，残存する未分化な細胞に対し特異的に細胞死を誘導することができ，のちに肝臓へと効率的に分化させることに成功した．未分化な過程におけるメチオニン除去培地の処理によるおのおのの胚葉への分化の促進は，各種の細胞を作製する期間の短縮および分化の効率化につながり，ヒトのES細胞およびiPS細胞を利用した創薬研究および再生医療に寄与できる．また，残存した未分化な細胞を除去することは，効率的な分化の誘導への利用のみならず，移植医療において，残存した未分化な幹細胞に由来するテラトーマの発生するリスクの低減に大きく寄与することが期待できる．今後は，ヒトのES細胞およびiPS細胞におけるメチオニン代謝と遺伝子の発現制御との関係性の解明が課題である．

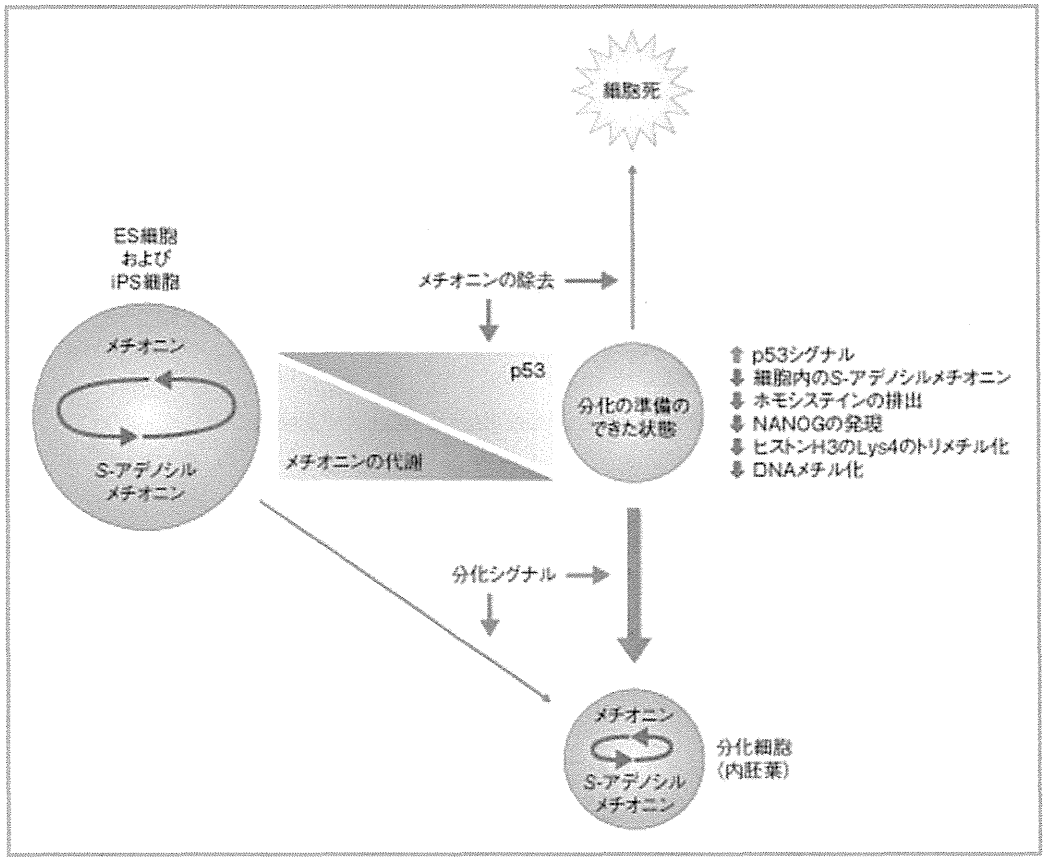

図2 ヒトのES細胞およびiPS細胞におけるメチオニン代謝の役割

ヒトのES細胞およびiPS細胞では，分化した内胚葉と比べメチオニン代謝がさかんであり，メチオニン除去培地で短期間培養すると細胞は一時的に分化しやすい状態になり，長時間培養すると細胞死が起こる．

[Download] http://first.lifesciencedb.jp/wp-content/uploads/2014/05/Kume-Cell-Metabolism-14.5.2-

Fig.2.jpg

文 献

1. Shiraki, N., Umeda, K., Sakashita, N. et al.: **Differentiation of mouse and human embryonic stem cells into hepatic lineages.** Genes Cells, 13, 731-746 (2008)[PubMed http://www.ncbi.nlm.nih.gov/pubmed/18513331]
2. Shiraki, N., Yoshida, T., Araki, K. et al.: **Guided differentiation of embryonic stem cells into Pdx1-expressing regional-specific definitive endoderm.** Stem Cells, 26, 874-885 (2008)[PubMed http://www.ncbi.nlm.nih.gov/pubmed/18238854]
3. Sakano, D., Shiraki, N., Kikawa, K. et al.: **VMAT2 identified as a regulator of late-stage β-cell differentiation.** Nat. Chem. Biol., 10, 141-148 (2014)[PubMed http://www.ncbi.nlm.nih.gov/pubmed/24316738] [新着論文レビュー http://first.lifesciencedb.jp/archives/8151]
4. Ogaki, S., Shiraki, N., Kume, K. et al.: **Wnt and Notch signals guide embryonic stem cell differentiation into the intestinal lineages.** Stem Cells, 31, 1086-1096 (2013)[PubMed http://www.ncbi.nlm.nih.gov/pubmed/23378042]
5. Facucho-Oliveira, J. M. & St. John, J. C.: **The relationship between pluripotency and mitochondrial DNA proliferation during early embryo development and embryonic stem cell differentiation.** Stem Cell Rev., 5, 140-158 (2009)[PubMed http://www.ncbi.nlm.nih.gov/pubmed/19521804]
6. Wellen, K. E. & Thompson, C. B.: **A two-way street: reciprocal regulation of metabolism and signalling.** Nat. Rev. Mol. Cell Biol., 13, 270-276 (2012)[PubMed http://www.ncbi.nlm.nih.gov/pubmed/22395772]
7. Takubo, K., Nagamatsu, G., Kobayashi, C. I. et al.: **Regulation of glycolysis by Pdk functions as a metabolic checkpoint for cell cycle quiescence in hematopoietic stem cells.** Cell Stem Cell, 12, 49-61 (2013)[PubMed http://www.ncbi.nlm.nih.gov/pubmed/23290136]
8. Wang, J., Alexander, P., Wu, L. et al.: **Dependence of mouse embryonic stem cells on threonine catabolism.** Science, 325, 435-439 (2009)[PubMed http://www.ncbi.nlm.nih.gov/pubmed/19589965]
9. Shyh-Chang, N., Locasale, J. W., Lyssiotis, C. A. et al.: **Influence of threonine metabolism on *S*-adenosylmethionine and histone methylation.** Science, 339, 222-226 (2013)[PubMed http://www.ncbi.nlm.nih.gov/pubmed/23118012]
10. Osafune, K., Caron, L., Borowiak, M. et al.: **Marked differences in differentiation propensity among human embryonic stem cell lines.** Nat. Biotechnol., 26, 313-315 (2008)[PubMed http://www.ncbi.nlm.nih.gov/pubmed/18278034]

著者プロフィール

白木 伸明(Nobuaki Shiraki)

略歴:2006年 熊本大学大学院医学研究科博士課程 修了, 2009年より熊本大学発生医学研究所 助教.

研究テーマ:内胚葉の発生および分化.

粂 昭苑(Shoen Kume)

熊本大学発生医学研究所 教授.

研究室URL:http://www.imeg.kumamoto-u.ac.jp/divisions/stem_cell_biology/

ジャーナル: Cell Metabolism | タグ: アミノ酸代謝・マウス・分子生物学・多能性幹細胞

1521-009X/42/11/1947–1954$25.00
DRUG METABOLISM AND DISPOSITION

http://dx.doi.org/10.1124/dmd.114.059493
Drug Metab Dispos 42:1947–1954, November 2014

Human Small Intestinal Epithelial Cells Differentiated from Adult Intestinal Stem Cells as a Novel System for Predicting Oral Drug Absorption in Humans

Toru Takenaka, Naomoto Harada, Jiro Kuze, Masato Chiba, Takahiro Iwao, and Tamihide Matsunaga

Discovery Drug Metabolism and Pharmacokinetics, Pharmacokinetics Research Laboratories (T.T., J.K., M.C.), and Evaluation Research Laboratory (N.H.), Tsukuba Research Center, Taiho Pharmaceutical Co. Ltd., Tsukuba, Ibaraki, Japan; and Department of Clinical Pharmacy, Graduate School of Pharmaceutical Sciences, Nagoya City University, Nagoya, Japan (T.I., T.M.).

Received June 16, 2014; accepted September 8, 2014

ABSTRACT

Adult intestinal stem cells (ISCs) possess both a long-term proliferation ability and differentiation capability into enterocytes. As a novel in vitro system for the evaluation of drug absorption, we characterized a human small intestinal epithelial cell (HIEC) monolayer that differentiated from adult ISCs. Continuous proliferation/differentiation from ISCs consistently conferred the capability of maturation of enterocytes to HIECs over 25 passages. The morphologically matured HIEC monolayer consisted of polarized columnar epithelia with dense microvilli, tight junctions, and desmosomes 8 days after seeding onto culture inserts. Transepithelial electrical resistance across the monolayer was 9-fold lower in HIECs (98.9 Ω × cm^2) than in Caco-2 cells (900 Ω × cm^2), which indicated that the looseness of the tight junctions in the HIEC monolayer was similar to that in the human small intestine (approximately 40 Ω × cm^2). No significant differences were observed in the overall gene expression patterns of the major drug-metabolizing enzymes and transporters between the HIEC and Caco-2 cell monolayers. Furthermore, the functions of P-glycoprotein and breast cancer resistance protein in the HIEC monolayer were confirmed by the vectorial transport of marker substrates and their disappearance in the presence of specific inhibitors. The apparent drug permeability values of paracellularly transported compounds (fluorescein isothiocyanate-dextran 4000, atenolol, and terbutaline) and nucleoside transporter substrates (didanosine, ribavirin, and doxifluridine) in the HIEC monolayer were markedly higher than those of Caco-2 cells, whereas transcellularly transported drugs (pindolol and midazolam) were equally well permeated. In conclusion, the HIEC monolayer can serve as a novel and superior alternative to the conventional Caco-2 cell monolayer for predicting oral absorption in humans.

Introduction

Oral absorption often needs to be predicted in humans to assess the feasibility of drug development so that development candidates can be selected and prioritized at the discovery stage. Many techniques have served as tools for the prediction of intestinal absorption and metabolism in humans. For example, Lennernäs et al. (1997) demonstrated that the human jejunal perfusion method could predict human oral absorption for both passively and carrier-mediated transported drugs. The Ussing-chamber model has also been used as a system that can not only accurately predict absorption, but can also evaluate metabolism (Rozehnal et al., 2012; Sjöberg et al., 2013). However, neither technique is frequently used as a routine assay at the discovery stage of new drug candidates because of the limited and irregular availability of human materials for these systems.

dx.doi.org/10.1124/dmd.114.059493.

Cell-based assay methods such as Caco-2 cells (human colon adenocarcinoma cells), MDCK cells (Madin–Darby canine kidney cells), and 2/4/A1 cells (conditionally immortalized rat intestinal cells) have also been used to evaluate membrane permeability and the transport of drug candidates (Irvine et al., 1999; Tavelin et al., 2003b; Skolnik et al., 2010). The Caco-2 cell line is one of the most widely used cell systems. Although the Caco-2 cell line retains very similar morphologic properties to human enterocytes, its tight junctions are markedly tighter than those in the small intestine, which may reduce the permeability of drugs with significant paracellular absorption (Lennernäs et al., 1996; Saitoh et al., 2004), thereby resulting in the underestimation of intestinal absorption for those compounds (Tavelin et al., 2003b; Saitoh et al., 2004; Matsson et al., 2005). The utilization of human primary normal enterocytes was expected to be a promising solution for the aforementioned discrepancy between in vivo and in vitro models. Although several methods have been used to isolate primary enterocytes from the human small intestine (Perreault and Beaulieu, 1998; Aldhous et al., 2001; Grossmann et al.,

ABBREVIATIONS: BCRP, breast cancer resistance protein; BrdU, bromodeoxyuridine; CDX2, caudal type homeobox 2; CNT, concentrative nucleoside transporter; Ct, threshold cycle; DMEM, Dulbecco's modified Eagle's medium; ENT, equilibrative nucleoside transporter; ER, efflux ratio; *F*a, fraction absorbed in humans; FBS, fetal bovine serum; FD-4, fluorescein isothiocyanate–dextran with an average molecular weight of 4000; HIEC, human small intestinal epithelial cell; IFABP, intestinal fatty acid-binding protein; iPS, induced pluripotent stem; ISC, intestinal stem cell; Ko143, 3-(6-isobutyl-9-methoxy-1,4-dioxo-1,2,3,4,6,7,12,12α-octahydropyrazino[1′,2′:1,6]pyrido[3,4-*b*]indol-3-yl)-propionic acid *tert*-butyl ester; LGR5, leucine-rich repeat-containing G protein–coupled receptor 5; MRP, multidrug resistance protein; P450, cytochrome P450; PAMPA, parallel artificial membrane permeability assay; P_{app}, apparent permeability coefficient, ; P-gp, P-glycoprotein; SI, sucrase-isomaltase; TEER, transepithelial electrical resistance; TM, transport medium; UGT, UDP-glucuronosyltransferase.

2003; Chougule et al., 2012), their applications remain limited, which has been attributed to their poor viability and short life span (Aldhous et al., 2001; Grossmann et al., 2003).

Adult stem cells are found in many organs, including the intestine, after development, and possess a long-term proliferation ability and differentiation capability into several distinct cell types. Therefore, adult stem cells are responsible for adult tissue homeostasis and the regeneration of damaged tissue. The small intestinal epithelium is rapidly self-renewed via cell proliferation and migration along the crypt-villus axis. This systematic process consists of the proliferation of adult intestinal stem cells (ISCs) at the bottom of the crypt, migration into the villi with differentiation/maturation, and eventual apoptosis at the tips of the villi (Yeung et al., 2011). Suzuki et al. (2010) recently reported that adult ISCs expressing leucine-rich repeat-containing G protein–coupled receptor 5 (LGR5), a marker of ISCs, were contained in commercially available primary normal human small intestinal epithelial cells (HIECs). The authors demonstrated that ISCs were maintained in culture with continuous proliferation and spontaneous differentiation into four distinct epithelial cell lineages including not only absorptive enterocytes, but also secretory lineages such as enteroendocrine cells, goblet cells, and Paneth cells. Suzuki et al. (2010) also found that these differentiated cells formed polarized monolayers with dome-like structures. However, to the best of our knowledge, the utility of this differentiated HIEC for evaluating the permeability of drug candidates to predict absorption in humans has not yet been assessed.

In this study, we characterized the HIEC monolayer as a novel tool for the evaluation of oral drug absorption. The HIEC had the ability to form a monolayer with a tight and matured in vivo–like morphology. HIECs also displayed the long-term proliferating ability of ISCs and continuous differentiation potency into enterocytes from ISCs. The looseness of tight junctions in the HIEC monolayer, which had a transepithelial electrical resistance (TEER) value of 98.9 $\Omega \times cm^2$, was similar to that of the human small intestine (TEER = approximately 40 $\Omega \times cm^2$) (Sjöberg et al., 2013), whereas that of Caco-2 cells was not (TEER = 900 $\Omega \times cm^2$). The HIEC monolayer also distinctly expressed concentrative nucleoside transporter (CNT) 3, which was absent in Caco-2 cells. As a result, the permeability values of paracellularly transported and nucleoside transporter substrates were markedly higher in the HIEC monolayer than in Caco-2 cells, whereas transcellularly transported drugs were equally well permeated. This study demonstrated that the HIEC monolayer could serve as a novel and superior alternative to the conventional Caco-2 cell monolayer for predicting oral absorption in humans; its accuracy was more pronounced for paracellularly transported drugs and nucleoside transporter substrates.

Materials and Methods

HIECs (ACBRI519) and Caco-2 cells (HTB-37) were obtained from Cell Systems (Kirkland, WA) and the American Type Culture Collection (Rockville, VA), respectively. Dulbecco's modified Eagle's medium (DMEM), DMEM mixed 1:1 with Ham's F-12 (DMEM/F12), 0.25% trypsin-EDTA, Hanks' balanced salt solution, nonessential amino acids, penicillin-streptomycin, and GlutaMAX were obtained from Life Technologies (Carlsbad, CA). Bovine pituitary extract was purchased from Kohjin Bio (Saitama, Japan). Fetal bovine serum (FBS) was obtained from SAFC Biosciences (Lenexa, KS). Recombinant human insulin, epidermal growth factor, and fluorescein isothiocyanate–dextran with an average molecular weight of 4000 (FD-4) were purchased from Sigma-Aldrich (St. Louis, MO). Fibrillar collagen–coated 24-well inserts were purchased from BD Gentest (Woburn, MA). Twelve-well transwell membrane inserts were obtained from Corning (Corning, NY). All compounds for the transport assay were purchased from Sigma-Aldrich, LKT Laboratories (St. Paul, MN), and Tokyo Kasei Kogyo (Tokyo, Japan). All other chemicals and reagents were of analytical grade.

Cell Culture. HIECs were maintained on type I collagen–coated culture dishes in DMEM/F-12 supplemented with 10% FBS, 1% GlutaMAX, 10 μM dexamethasone, 1 μg/ml insulin, 20 ng/ml epidermal growth factor, 50 μM 2-mercaptoethanol, 50 U/ml penicillin, and 50 μg/ml streptomycin. Caco-2 cells were grown on culture flasks in DMEM with 4.5 g/l glucose, supplemented with 10% FBS, 1× nonessential amino acids, 1× GlutaMAX, 50 U/ml penicillin, and 50 μg/ml streptomycin. Both cell lines were cultured at 37°C in a humidified atmosphere of 5% CO_2 and 95% air. Before reaching confluence (every 4 to 5 days), HIECs and Caco-2 cells were treated with 0.25% trypsin-EDTA, and subcultured at a split ratio of 1:4, or seeded at 1×10^5 cells/well onto 24-well fibrillar collagen–coated inserts and at 6.3×10^4 cells/well onto 12-well noncoated membrane inserts, respectively. HIECs were fed tridaily with culture medium, supplemented with 50 μg/ml bovine pituitary extract. The culture medium for Caco-2 cells was replaced once in the first week and every other day thereafter. HIECs and Caco-2 cells were grown for 8 to 9 days and 18–20 days, respectively, before assays were performed. TEER values were measured to check the integrity of the monolayer using Millicell-ERS (Millipore, Bedford, MA).

Proliferation Analysis. HIECs were seeded on type I collagen–coated 96-well plates at 5×10^3 cells/well. Cell proliferation analysis was performed 48 hours after seeding by using a colorimetric bromodeoxyuridine (BrdU) cell proliferation assay kit (Millipore) according to the manufacturer's instructions. A cell viability assay was also performed 48 hours after seeding by using Cell Counting Kit-8 (Dojindo, Kumamoto, Japan). BrdU incorporation into the DNA of proliferating cells as well as cell viability were measured with a microplate reader (SpectraMax Gemini; Molecular Devices, Sunnyvale, CA) at 450 nm with a reference wavelength of 650 nm. To compensate for variability of viable cell numbers, the absorbance in the BrdU incorporation assay was divided by the absorbance in the cell viability assay.

mRNA Quantification. Total RNA was extracted using the PureLink RNA Mini Kit (Life Technologies) from HIECs and Caco-2 cells on 8 and 20 days, respectively, after cell seeding onto membrane inserts. Total RNA from subconfluent HIECs was also extracted in the same manner. These total RNAs and human small intestinal total RNA (5-donor pooled; BioChain Institute, Newark, CA) were used to prepare cDNA using the PrimeScript RT reagent kit (Takara; Shiga, Japan). The quantitative real-time polymerase chain reaction amplification of cDNA corresponding to 25 ng of total RNA was performed in a reaction mixture (20 μl) containing 1× concentration of FAST SYBR Green Master Mix (Applied Biosystems, Foster City, CA) and 0.2 μM primer pairs (Table 1) for caudal type homeobox 2 (CDX2), intestinal fatty acid-binding protein (IFABP), apical sodium-dependent bile acid transporter, monocarboxylate transporter 1, and multidrug resistance protein (MRP) 3, or containing 1× concentration of the TaqMan fast universal PCR master mix (Applied Biosystems) and the following TaqMan Gene Expression Assay with individual assay IDs: LGR5 (Hs00173664_m1), sucrase-isomaltase (SI) (Hs00356112_m1), CNT1 (Hs00984403_m1), CNT2 (Hs00188407_m1), CNT3 (Hs00910439_m1), equilibrative nucleoside transporter (ENT) 1 (Hs01085704_g1), ENT2 (Hs00155426_m1), ENT3 (Hs00217911_m1), and glyceraldehyde-3-phosphate dehydrogenase (Hs02758991_g1) on a 7500 FAST Real-Time PCR system (Applied Biosystems). Thermal cycling conditions included 95°C for 20 seconds, 40 cycles of 95°C for 3 seconds, and 60°C for 30 seconds. Threshold cycle (Ct) values were determined with 7500 software (Applied Biosystems). Ct values for target genes

TABLE 1

Sequences of primers for mRNA quantification

Gene	Primer Sequences (5′-3′)
CDX2	
Forward	ACCTGTGCGAGTGGATGC
Reverse	TCCTTTGCTCTGCGGTTCT
IFABP	
Forward	ACAATCTAGCAGACGGAACT
Reverse	TTGGCTTCTACTCCTTCATA
ASBT	
Forward	TGGCCCCAAAAAGCAAA
Reverse	AACCGTTCGGCACCTGTAC
MCT1	
Forward	CCGCGCATATAACGATATTT
Reverse	ATCCAACTGGACCTCCAA
MRP3	
Forward	GTCCGCAGAATGGACTTGAT
Reverse	TCACCACTTGGGGATCATTT

ASBT, apical sodium-dependent bile acid transporter; MCT1, monocarboxylate transporter 1.

were normalized to the Ct value of glyceraldehyde-3-phosphate dehydrogenase (ΔCt). Relative mRNA expression was determined using the $2^{-\Delta\Delta Ct}$ method. We selected Ct values > 35 as the cut-off for the absence of expression.

The mRNA levels of other transporters, including organic cation transporter 1, organic anion-transporting peptide 2B1, P-glycoprotein (P-gp), breast cancer resistance protein (BCRP), and MRP1 and MRP2, and the drug-metabolizing cytochrome P450 (P450) enzymes CYP2C9, CYP2C19, CYP2D6, CYP3A4, and CYP3A5, and UDP-glucuronosyltransferases (UGTs) UGT1A1, UGT1A3, UGT1A4, UGT1A6, and UGT2B7 were analyzed using the QuantiGene Plex 2.0 Assay Kit (Affymetrix, Santa Clara, CA) according to the manufacturer's instructions. HIECs and Caco-2 cells cultured on membrane inserts for 8 and 20 days, respectively, were lysed with the QuantiGene Sample Processing Kit (Affymetrix). Samples were analyzed using a Bio-Plex 200 suspension array system (Bio-Rad, Hercules, CA). The expression level of hypoxanthine phosphoribosyltransferase was used to normalize mRNA expression data from the target genes.

Transmission Electron Microscopy of HIECs. HIECs seeded on culture inserts as described above were fixed with 2% paraformaldehyde and 2% glutaraldehyde in 0.1 M phosphate buffer (pH 7.4) and were then cooled to 4°C. Thereafter, they were fixed with 2% glutaraldehyde in 0.1 M phosphate buffer (pH 7.4) at 4°C overnight. After three washes with 0.1 M phosphate buffer, cells were postfixed with 2% osmium tetroxide in 0.1 M phosphate buffer at 4°C for 90 minutes, and dehydrated through a graded ethanol series (50–100%). The samples were embedded in resin, and ultrathin sections were stained with 2% uranyl acetate and lead stain solution. The specimens were examined using a JEM-1200 EX transmission electron microscope (JEOL, Tokyo, Japan).

Transport Assay. Prior to the addition of substrates, growth medium was removed and monolayers were rinsed twice with transport medium (TM) (Hanks' balanced salt solution with 4.2 mM $NaHCO_3$ and 20 mM glucose) adjusted to pH 7.4 by 10 mM HEPES. Monolayers were preincubated in TM (pH 7.4) for 30 minutes at 37°C in 95% humidity. Transport assays were carried out with apical and basal buffers consisting of TM adjusted to pH 6.5 by 10 mM MES and TM (pH 7.4) with 4.5% (w/v) bovine serum albumin, respectively. The following buffer volumes were used for the apical and basal chambers: 0.4 ml and 1.2 ml, respectively, for HIECs; and 0.5 ml and 1.5 ml, respectively, for Caco-2 cells. Donor concentrations for the different test compounds were set at 50 μM, except for didanosine (100 μM), ribavirin (100 μM), doxifluridine (100 μM), and FD-4 (500 μg/ml) due to low quantification sensitivity. Monolayers were incubated for 120 minutes at 37°C in 95% humidity with 80 rpm reciprocal shaking. Basal compartments were sampled at 30, 60, and 120 minutes. Except for topotecan, samples were added to twice its volume of methanol/acetonitrile (2:1, v/v) and centrifuged for 15 minutes at 10,000*g* before being analyzed with a liquid chromatography–tandem mass spectrometry system. Regarding topotecan, twice the volume of methanol/7% perchloric acid (1:1, v/v) was added to samples instead of methanol/acetonitrile (2:1, v/v) to quantify the total of its lactone form and carboxylated form (Rosing et al., 1995). TEER values were measured to check the integrity of the monolayer and the influence of the test compounds on cells before and after the experiment. No significant decreases were observed in TEER values during the transport assays in any of the experiments.

Bidirectional Transport Assay. Digoxin and mitoxantrone were chosen as substrates to examine the functions of P-gp and BCRP, respectively. Verapamil (10 μM) and Ko143 (5 μM) [3-(6-isobutyl-9-methoxy-1,4-dioxo-1,2,3,4,6,7,12,12α-octahydropyrazino[1′,2′:1,6]pyrido[3,4-*b*]indol-3-yl)-propionic acid *tert*-butyl ester] were used as the specific inhibitors of P-gp and BCRP, respectively. The bidirectional transport assays were conducted as described above with the exceptions that the TM at pH 7.4 with or without inhibitors was used for both the donor and acceptor chambers. Before the experiment, the monolayers were preincubated for 30 minutes with TM (pH 7.4) containing inhibitors or vehicle. The initial concentrations of digoxin and mitoxantrone were 10 and 20 μM, respectively.

Transport Assay Using Artificial Membranes. The drug permeability assay through an artificial membrane was conducted using a precoated parallel artificial membrane permeability assay (PAMPA) plate system (BD Gentest) in accordance with the manufacturer's instructions. Briefly, 300 μl of test compounds in PBS (pH 6.5) and 200 μl PBS (pH 7.4) were added into the donor and acceptor wells, respectively. After incubation at 37°C for 4 hours, the concentrations of test compounds were measured in both the donor and acceptor wells. The initial donor concentrations for the test compounds were the same as those used for the transport assays in the HIEC and Caco-2 cell monolayers.

Sample Analysis. An analysis of samples was performed using the liquid chromatography–tandem mass spectrometry system, which consisted of a Waters Quattro Micro Mass Spectrometer and Waters Alliance 2795 HT (Waters, Milford, MA), except for FD-4. The ionization source was an electrospray. The multiple-reaction monitoring mode was used to monitor ions as follows: digoxin (779.1 > 649.2), mitoxantrone (445.3 > 88.0), vinblastine (811.3 > 224.1), topotecan (422.0 > 171.0), didanosine (237.1 > 137.0), atenolol (267.2 > 145.0), terbutaline (226.2 > 152.0), ribavirin (245.0 > 112.9), doxifluridine (245.0 > 171.0), pindolol (249.2 > 116.0), midazolam (326.0 > 222.7), 1′-hydroxymidazolam (341.9 > 323.9), and 4-hydroxymidazolam (342.0 > 324.9). The Cosmosil 5C18 AR-II column (50 mm, 4.6 mm i.d.; Nacalai Tesque, Kyoto, Japan) was used for the chromatographic separation of analytes for digoxin, mitoxantrone, vinblastine, topotecan, atenolol, terbutaline, pindolol, midazolam, 1′-hydroxymidazolam, and 4-hydroxymidazolam. The Capcellpak C18 AQ column (150 mm, 4.6 mm i.d.; Shiseido, Tokyo, Japan) was used for the chromatographic separation of analytes for didanosine, ribavirin, and doxifluridine. The following gradient condition was used for the elution of digoxin, mitoxantrone, vinblastine, topotecan, didanosine, terbutaline, ribavirin, doxifluridine, pindolol, midazolam, 1′-hydroxymidazolam, and 4-hydroxymidazolam: at 0, 1.5, 4, 4.1, and 8.5 minutes, the percentages of acetonitrile were 2, 95, 95, 2, and 2, respectively, with 0.1% formic acid as the aqueous mobile phase. The gradient condition for atenolol was as follows: at 0, 1.5, 3, 3.1, and 8 minutes, the percentages of methanol were 5, 80, 80, 5, and 5, respectively, with 10 mM ammonium acetate as the aqueous mobile phase. The flow rate was 0.2 ml/min and the injection volume was 5 μl. Column temperatures were maintained at 40°C. All data processing was performed with Waters QuanLynx software (Waters, Woburn, MA).

The concentrations of FD-4 were measured using a fluorescence microplate reader at excitation and emission wavelengths of 490 and 520 nm, respectively (SpectraMax Gemini; Molecular Devices).

Calculations. The apparent drug permeability (P_{app}) was calculated for cellular transport in the HIEC and Caco-2 cell monolayers according to eq. 1 by using the linear part of the time versus transported amount:

$$P_{app} = \frac{dQ}{dt} \times \frac{1}{A \times C_0} \quad (1)$$

where dQ/dt, A, and C_0 represent the total amount of the test compound transported to the acceptor chamber per unit time, the surface area of the transport membrane (0.33 and 1 cm^2 for HIECs and Caco-2 cells, respectively), and the initial compound concentration in the donor chamber, respectively.

The efflux ratio (ER) was determined from the ratio of P_{app} in secretory (basal-to-apical) to that in absorptive (apical-to-basal) directions.

The P_{app} for the PAMPA assay was calculated using eq. 2:

$$P_{app} = -\ln\left(1 - C_A \times \frac{V_D + V_A}{C_D \times V_D + C_A \times V_A}\right) \div \left[A \times \left(\frac{1}{V_D} + \frac{1}{V_A}\right) \times t\right] \quad (2)$$

where C_D and C_A represent the final concentrations in the donor and acceptor wells, respectively; V_D and V_A represent the volumes of the donor and acceptor wells, respectively; and A and t represent the membrane surface area (0.3 cm^2) and incubation time, respectively.

The relationship between the P_{app} values and known fraction absorbed in humans (Fa) data were described using eq. 3 (Amidon et al., 1988):

$$Fa = 100 \times \left(1 - \exp\left(-a \times P_{app}\right)\right) \quad (3)$$

where a is the scaling factor. The best fitting curves were calculated by nonlinear regression using XLfit software (IDBS, Guildford, UK).

Results

Morphology of HIECs. HIECs survived and proliferated under our culture condition as previously demonstrated (Suzuki et al., 2010), and formed domes, which were similar to those in Caco-2 cells, after confluence on culture dishes (Fig. 1A). As monolayers were formed in HIECs and Caco-2 cells, TEER values increased and reached plateaus at

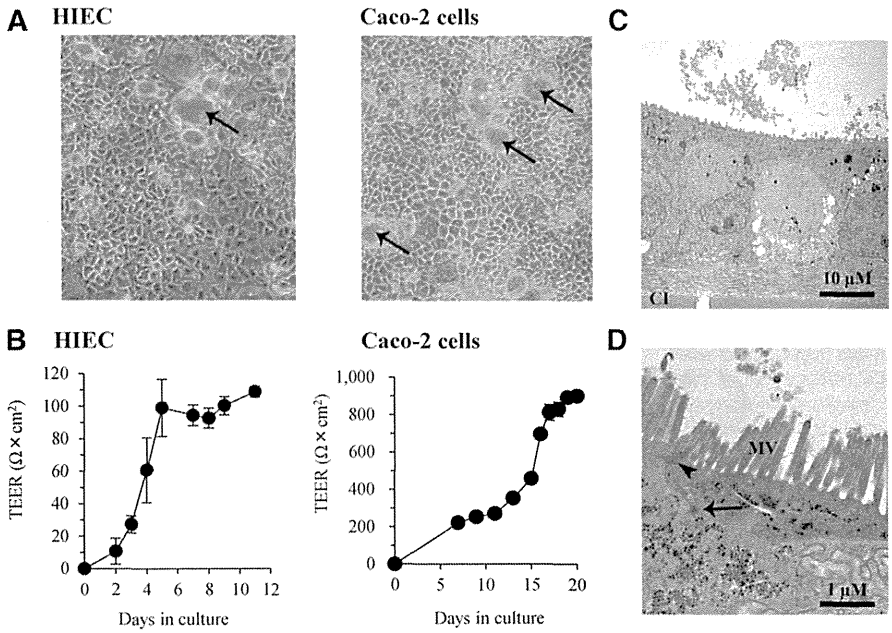

Fig. 1. Morphology and monolayer formation of HIECs and Caco-2 cells. (A) Phase contrast microscopies of HIECs and Caco-2 cells on culture dishes. Arrow, dome-like structure. Original magnification, 40×. (B) TEER values versus days in culture in HIECs and Caco-2 cells monolayers. TEER measurements were conducted in the culture medium. The data shown represent the mean ± S.D. (n = 3). (C and D) Transmission electron microscopy of HIECs grown on culture inserts. Monolayers composed of polarized columnar-shaped cells (C) with junctional complexes (tight junction and desmosome) and dense tall microvilli (D). Arrowhead, tight junction; arrow, desmosome. CI, culture insert; MV, microvilli. Bar, 10 μm in C; 1 μm in D.

98.9 ± 17.5 Ω × cm^2 on day 5 and at 900 ± 23 Ω × cm^2 on day 20 after seeding of HIECs and Caco-2 cells, respectively (Fig. 1B). The TEER values remained on a plateau at least until day 11 in the HIEC monolayer, and the value in the HIEC monolayer was more than 9-fold lower than that in the differentiated Caco-2 cell monolayer.

In agreement with these results, transmission electron microscopy confirmed the morphologic maturation of the HIEC monolayers after 8 days of growth on culture inserts (Fig. 1, C and D). HIECs grew as monolayers of polarized columnar epithelia (Fig. 1C) with straight dense microvilli, tight junctions, and desmosomes being observed under a higher magnification (Fig. 1D). These results indicated that HIECs differentiated into enterocytes with morphologically mature characteristics under our culture condition.

Long-Term Proliferation Ability, Maintained Population of ISCs, and Differentiation Potency into Enterocytes. Under our culture conditions, HIECs constantly proliferated over 25 passages without reaching senescence (Fig. 2A), which implied that ISCs continuously existed and underwent cell division, leading to a long-term proliferating ability and formation capability of HIEC monolayers. To confirm this hypothesis, we examined the mRNA expression levels of CDX2 and LGR5, a hindgut marker and an ISC marker (Barker and Clevers, 2010; Iwao et al., 2014), respectively, at various passages. The mRNA expression levels of CDX2 and LGR5 at subconfluence remained almost constant up to 25 passages (Fig. 2B). In addition, there was no consistent pattern of change in LGR5 levels between subconfluence and day 8 after seeding on culture inserts. These results indicated that the markedly high number of ISCs was maintained over a long period of time, even after the formation of monolayers. Differentiation potency into enterocytes was also examined by measuring the mRNA expression levels of IFABP and SI, markers for differentiated enterocytes (Levy et al., 2009; Suzuki et al., 2010; Iwao et al., 2014) (Fig. 2C). The increase observed in the expression levels of IFABP and SI on day 8 after seeding at any passage number indicated that ISCs had retained the potential to be differentiated into enterocytes. Moreover, the integrity of the HIEC monolayer during serial passage was examined by measuring TEER values (Fig. 2D). The TEER values of HIEC monolayers on day 8 after seeding were almost constant over the passage numbers tested, which suggested that HIECs formed monolayers with equal tightness over long-term continuous passages.

mRNA Analysis of Drug-Metabolizing Enzymes and Transporters. The gene expression profiles of drug-metabolizing enzymes and transporters in HIECs and Caco-2 cells are summarized in Fig. 3. The mRNA expression levels of CYP3A5, UGT1A3, UGT1A6, organic cation transporter 1, organic anion-transporting peptide 2B1, monocarboxylate transporter 1, CNT3, ENT1, ENT2, ENT3, P-gp, BCRP, MRP1, MRP2, and MRP3 in HIECs were within 10-fold of those in the human small intestine, whereas those of other P450/UGT isoforms and transporters in HIECs were markedly lower (<10%) than those in the human small intestine. UGT1A6 and CNT3 mRNA expression levels were 6-fold and 17-fold higher in the HIEC monolayer than in Caco-2 cells, respectively, whereas the mRNA expression levels of CYP2C9, CYP2C19, UGT2B7, and apical sodium-dependent bile acid transporter in Caco-2 cells were >17-fold higher than those in HIECs. CYP3A4, UGT1A1, UGT1A4, and CNT1 mRNA expression levels in both HIECs and Caco-2 cells were < 7.0% of those in the human small intestine. Among the mRNAs for transporters tested, CNT2 was not detected (Ct > 35) in either monolayers in this study.

Bidirectional Transport across HIEC and Caco-2 Cell Monolayers. Bidirectional (apical-to-basal and basal-to-apical) permeability coefficients for digoxin, a P-gp marker substrate (Pauli-Magnus et al., 2000), and mitoxantrone, a BCRP marker substrate (Matsson et al., 2009), were determined in both HIEC and Caco-2 cell monolayers to examine the functions of efflux transport mediated by these transporters. The values of ER, calculated from the ratio of P_{app} in secretory (basal-to-apical) to that in absorptive (apical-to-basal) directions, of digoxin in HIEC and Caco-2 cells were 2.2 and 3.1, respectively (Fig. 4A). In addition, verapamil, a P-gp inhibitor (Pauli-Magnus et al., 2000), reduced the ER value to almost 1 in both monolayers. Regarding BCRP-mediated transport, mitoxantrone was transported with markedly larger ER values in HIEC (ER = 38.2) than in Caco-2 cells (ER = 4.0) (Fig. 4B). The ER values of mitoxantrone in both cells were reduced by

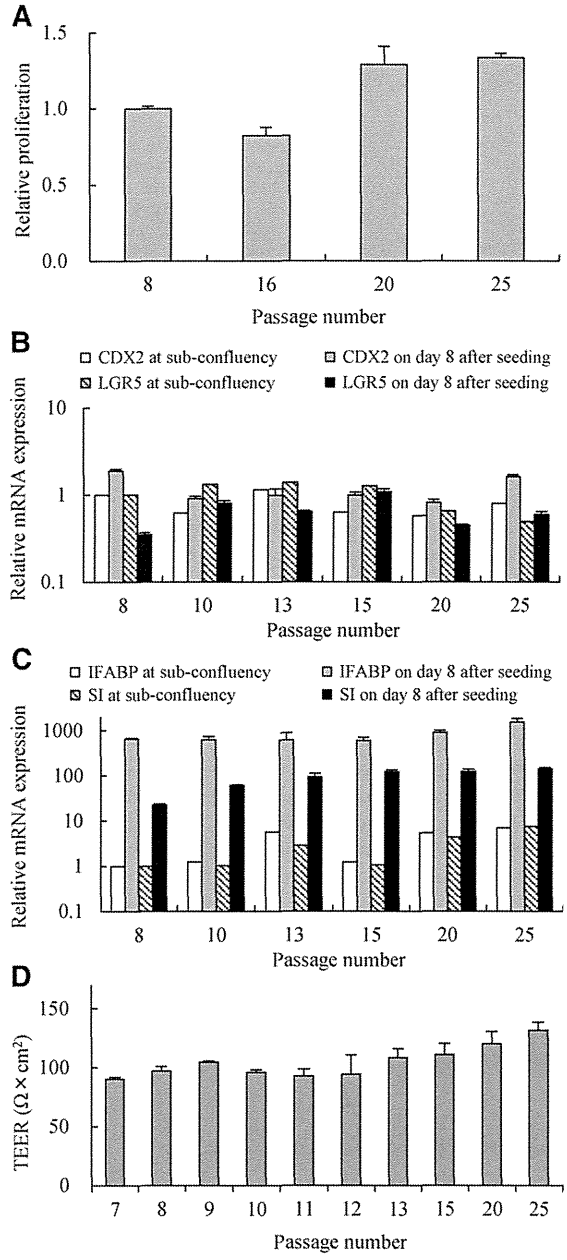

Fig. 2. Long-term proliferation ability, maintained population of ISCs, and differentiation potency into enterocytes. (A) Effect of the passage number on the relative cell proliferation activity. Data were represented as relative value to that at passage number 8. Data represent the mean ± S.D. (n = 6). (B and C) Effects of the passage number and culture time on the relative expression levels of CDX2, LGR5, IFABP, and SI. Quantitative real-time polymerase chain reaction analyses were performed with total RNA derived from HIECs at subconfluence and on day 8 after seeding onto culture inserts. The expression levels of each gene were normalized to those of glyceraldehyde-3-phosphate dehydrogenase, and are represented as the ratios of expression levels at subconfluence or on day 8 at various passage numbers to those at subconfluence at passage number 8. Data represent the mean ± S.D. (n = 3), except for the data at subconfluence. (D) Effects of the passage number on TEER values in HIEC monolayers. TEER measurements were conducted in culture medium on day 8 after seeding. Data represent the mean ± S.D. (n = 3).

Ko143, a specific BCRP inhibitor (Matsson et al., 2009). These results indicated that these efflux transporters were functionally active in the HIEC monolayer, similar to that in Caco-2 cells.

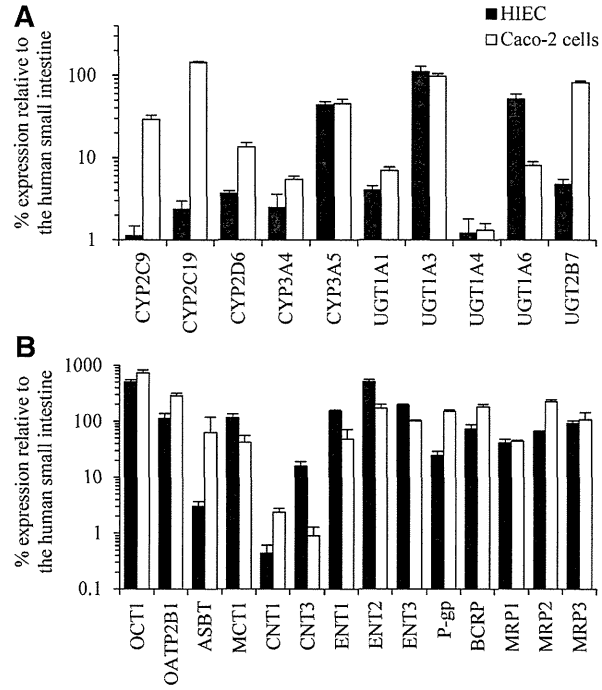

Fig. 3. Relative mRNA expression levels of drug-metabolizing enzymes (A) and transporters (B) in HIECs and Caco-2 cells. Expression levels were normalized to those of glyceraldehyde-3-phosphate dehydrogenase or hypoxanthine phosphoribosyltransferase, and are represented as relative values (%) to the human small intestine. Data represent the mean ± S.D. (n = 3). ASBT, apical sodium-dependent bile acid transporter; MCT1, monocarboxylate transporter 1; OATP2B1, organic anion-transporting peptide 2B1; OCT1, organic cation transporter 1.

Permeability of 10 Test Compounds across HIEC and Caco-2 Cell Monolayers and PAMPA. The P_{app} values for 10 test compounds across the HIEC and Caco-2 cell monolayers and in PAMPA are listed in Table 2. The compounds tested included those with diverse characteristics for intestinal absorption, such as the Fa, major route for absorption (paracellular versus transcellular), transporters involved in net absorption (P-gp, BCRP, and nucleoside transporters), and physicochemical properties (molecular weight, partition coefficient, and polar surface area). The P_{app} values of 10 test compounds in HIECs, Caco-2 cells, and PAMPA ranged from 0.56×10^{-6} to 30×10^{-6} cm/s, 0.035×10^{-6} to 170×10^{-6} cm/s, and 0.0046×10^{-6} to 40×10^{-6} cm/s, respectively. Transcellularly absorbed drugs (pindolol and midazolam) showed similarly high P_{app} values in all three models: 2.2×10^{-6} to 7.9×10^{-6} cm/s for pindolol and 30×10^{-6} to 170×10^{-6} cm/s for midazolam. The formation of the primary metabolites of midazolam (1′-hydroxymidazolam and 4-hydroxymidazolam) was less than the lower limit of quantification (3 nM) in the apical and basal buffers after a 2-hour incubation in both HIECs and Caco-2 cells, which was consistent with the low mRNA expression of CYP3A4 (Fig. 3). In agreement with the looseness of the tight junction in the HIEC monolayer being lower, as demonstrated by the lower TEER value than that of the Caco-2 monolayer (Fig. 1B), the P_{app} values for paracellularly absorbed compounds (FD-4, atenolol, and terbutaline) in the HIEC monolayer were markedly higher than those in both the Caco-2 monolayer and PAMPA. Possibly due to the higher expression levels of nucleoside transporters (CNT3, ENT1, ENT2, and ENT3) in HIECs than in Caco-2 cells (Fig. 3), didanosine, ribavirin, and doxifluridine, all substrates of nucleoside transporters, permeated more than 5-fold, 45-fold, and 24-fold faster, respectively, across the HIEC monolayer than the Caco-2 monolayer and by more

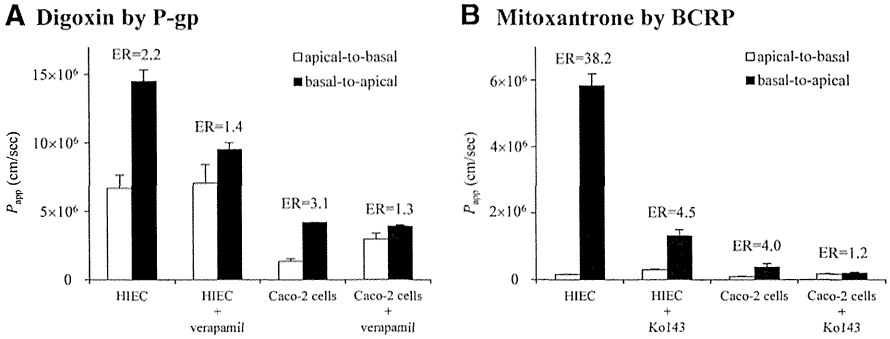

Fig. 4. Bidirectional permeability for digoxin and mitoxantrone across HIEC and Caco-2 cell monolayers in the presence or absence of inhibitors. (A) Efflux transport of digoxin (a P-gp substrate) in the presence or absence of verapamil. (B) Efflux transport of mitoxantrone (a BCRP substrate) in the presence or absence of Ko143. Data represent the mean ± S.D. (n = 3).

than 6-fold, 137-fold, and 34-fold faster, respectively, than PAMPA. PAMPA had the highest permeability for vinblastine (a P-gp substrate) and topotecan (a BCRP substrate) among assay systems tested, which was consistent with the lack of both P-gp and BCRP in PAMPA. The sigmoidal relationship between the P_{app} values of 10 test compounds and the Fa values were observed in HIECs and Caco-2 cells, but not in PAMPA (Fig. 5). The correlation coefficient in HIECs (0.779) was higher than that in Caco-2 cells (0.373).

Discussion

In this study, we showed that the HIEC monolayer, which differentiated from ISCs, displayed mature morphologic features consisting of polarized columnar epithelia with dense microvilli, tight junctions, and desmosomes. The looseness of the tight junctions in the HIEC monolayer was similar to that in the human small intestine, whereas those of Caco-2 cells were not, and the HIEC monolayer also had a high P_{app} for paracellularly absorbed compounds. Furthermore, the presence of the functions of P-gp and BCRP, and abundant mRNA expression of CNT3 made HIECs a valuable tool for studies on the intestinal absorption of these substrates.

Paracellular absorption refers to permeation across cell monolayers through pores in the tight junction, and the oral absorption of hydrophilic molecules generally relies on the paracellular pathway. In this study, the permeability values of paracellularly absorbed compounds (FD-4, atenolol, and terbutaline) were higher in HIECs than in Caco-2 cells (Table 2). These results indicated that the HIEC monolayer had a leakier paracellular route than Caco-2 cells. Furthermore, the permeability for these compounds of PAMPA, which completely lacks a paracellular pathway, was even lower. This result was consistent with the lower TEER value in the HIEC monolayer (98.9 $\Omega \times cm^2$) than in Caco-2 cells (900 $\Omega \times cm^2$) (Fig. 1). TEER values in the human duodenum, jejunum, and ileum have been reported to be 45, 34, and 37 $\Omega \times cm^2$, respectively (Sjöberg et al., 2013), and indicate that the TEER value of HIECs was closer to the human small intestine than that of Caco-2 cells. Previous studies reported that the oral absorption of compounds that permeate via the paracellular route was poorly predicted in the Caco-2 monolayer, and this was attributed to its excessively tight junctions (Tavelin et al., 2003b; Saitoh et al., 2004; Matsson et al., 2005). The monolayer of 2/4/A1 cells, conditionally immortalized rat intestinal cells, has been reported to possess a radius of tight junction pores and TEER value that are similar to those of the human small intestine (Tavelin et al., 1999, 2003a). These HIEC-like characteristics led to the similarly high P_{app} values of paracellularly absorbed drugs between the 2/4/A1 cell monolayer and human jejunum (Tavelin et al., 1999, 2003b). However, in contrast with HIECs, the activities of efflux transporters, such as P-gp, BCRP, and MRP, are completely absent in 2/4/A1 cells (Tavelin et al., 2003a). Therefore, the utility of the HIEC monolayer as a superior alternative to the 2/4/A1 cell monolayer remains to be confirmed by side-by-side comparisons with diverse compounds including paracellularly absorbed compounds and the substrates of these efflux transporters.

The permeability of the HIEC monolayer to didanosine, ribavirin, and doxifluridine, substrates of multiple nucleoside transporters (CNT2,

TABLE 2

P_{app} coefficients across monolayers (HIECs and Caco-2 cells) and in the PAMPA for the 10 test compounds

P_{app} values represent the mean ± S.D. (n = 3).

Compound	Fa[a]	P_{app}			Major Route for Absorption or Transporter	MolecularWeight	LogP[b]	PSA[b]
		HIECs	Caco-2 Cells	PAMPA				
	%	× 10^{-6} cm/s						$Å^2$
FD-4	0	0.56 ± 0.01	0.035 ± 0.009	0.0046 ± 0.0017	Paracellular	4000	—	—
Vinblastine	25	2.6 ± 0.1	0.57 ± 0.02	4.1 ± 0.8	Transcellular/P-gp	811.0	3.7	154.1
Topotecan	30	0.78 ± 0.14	0.35 ± 0.06	1.5 ± 0.1	Transcellular/BCRP	421.4	0.8	103.2
Didanosine	42	0.62 ± 0.12	0.11 ± 0.02	0.11 ± 0.01	Nucleoside transporters	236.2	−1.2	88.7
Atenolol	50	0.68 ± 0.09	0.34 ± 0.05	0.022 ± 0.005	Paracellular	266.3	0.2	84.6
Terbutaline	62	0.70 ± 0.05	0.069 ± 0.006	0.014 ± 0.001	Paracellular	225.3	0.9	72.7
Ribavirin	85	4.1 ± 0.3	0.092 ± 0.003	0.030 ± 0.002	Nucleoside transporters	244.2	−1.9	143.7
Doxifluridine	90	4.7 ± 0.6	0.20 ± 0.03	0.14 ± 0.03	Nucleoside transporters	246.2	−1.4[c]	99.1[d]
Pindolol	90	7.9 ± 0.7	3.6 ± 0.3	2.2 ± 0.1	Transcellular	248.3	1.8	57.3
Midazolam	100	30 ± 3	170 ± 7	40 ± 4	Transcellular	325.8	3.1[e]	30.2

LogP, partition coefficient; PSA, polar surface area.

[a]Fa values were obtained from published data (Yamashita et al., 2000; Sugano et al., 2002; Tavelin et al., 2003b; Dixit and Perelson, 2006; Skolnik et al., 2010; Varma et al., 2010; Lin et al., 2011; Sjöberg et al., 2013).

[b]Data obtained from www.drugbank.ca.

[c]Data obtained from the interview form of Furtulon capsules.

[d]Data obtained from http://pubchem.ncbi.nlm.nih.gov/.

[e]Data obtained from a reference (Rodgers and Rowland, 2006).

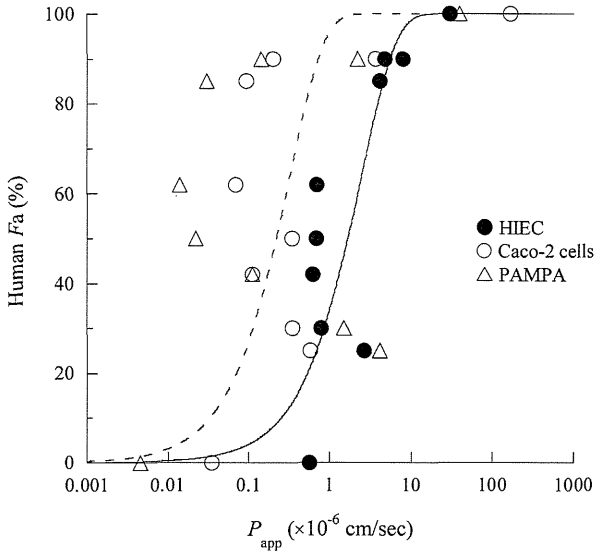

Fig. 5. Correlation between the *F*a values of 10 test compounds and the P_{app} values across HIECs, Caco-2 cells, and PAMPA. Solid and dashed lines represent the fitting curves obtained by eq. 3 for HIECs and Caco-2 cells, respectively. Data represent the mean of three independent monolayers.

CNT3, ENT2, and ENT3 for didanosine; CNT2, CNT3, ENT1, and ENT2 for ribavirin; CNT1, CNT3, ENT1, and ENT2 for doxifluridine) (Mangravite et al., 2003; Yamamoto et al., 2007; Zhang et al., 2007; Young et al., 2013) was considerably higher than that of Caco-2 cells and PAMPA (Table 2). Na^+-dependent CNTs and Na^+-independent ENTs are expressed in the human small intestine (Meier et al., 2007). Nucleosides and their analog drugs generally have hydrophilic properties and diffuse slowly across the cell membrane; therefore, nucleoside transporters expressed in the small intestine largely contribute to their oral absorption (Endres et al., 2009; Okayama et al., 2012; Ishida et al., 2013). Previous studies reported that Caco-2 cells did not express CNT1, CNT2, or CNT3 (Ward and Tse, 1999; Bourgine et al., 2012), which was consistent with the very low expression of CNTs observed in our study (Fig. 3B). In contrast with the Caco-2 monolayer, the significantly high expression of CNT3 mRNA (16% of human small intestine) in HIECs may have conferred an absorption capability for didanosine, ribavirin, and doxifluridine to the HIEC monolayer (Table 2). Ribavirin and doxifluridine, which are good substrates for CNT3 (Hu et al., 2006), had higher P_{app} values than didanosine, a relatively poor substrate for CNT3 (Hu et al., 2006), in the HIEC monolayer, and the rank order of their P_{app} values was in agreement with that of *F*a values.

Directional transport by P-gp and BCRP was confirmed in the HIEC monolayer by the efflux transport of the corresponding selective substrates (digoxin and mitoxantrone, respectively) and decreases in vectorial transport in the presence of specific inhibitors (verapamil and Ko143, respectively) (Fig. 4). Therefore, the HIEC monolayer can serve as a useful in vitro tool for the evaluation of P-gp– and BCRP–mediated transport during the absorption process. The ratio of P_{app} for the basal-to-apical direction to that for the apical-to-basal direction (ER) of mitoxantrone was approximately 10-fold higher in HIECs (38.2) than in Caco-2 cells (4.0) despite the lower mRNA expression of BCRP in HIECs than in Caco-2 cells (Fig. 3B). Ohtsuki et al. (2012) reported that the protein levels of several transporters including BCRP in the plasma membrane did not correlate with the respective mRNA levels in the human liver, and suggested that a post-transcriptional process and/or intracellular trafficking may play a key role in regulating the functional protein levels of transporters.

The overall lower expression profiles of drug-metabolizing enzymes in Caco-2 cells than in the human small intestine (Fig. 3) have been well documented in previous studies (Schmiedlin-Ren et al., 1997; Sun et al., 2002; Bourgine et al., 2012). In this study, the expression profile of mRNA for the P450/UGT isoforms in HIECs was similar to that in Caco-2 cells, except for CYP2C9, CYP2C19, UGT1A6, and UGT2B7. Although the causes of these exceptions are not known, the differences of origins (normal versus tumoral tissue) between HIECs and Caco-2 cells (Bourgine et al., 2012) and medium additives, such as insulin (Martínez-Jiménez et al., 2006) and dexamethasone (Jemnitz et al., 2002), may contribute these observations. Among the mRNAs whose expression was examined, the mRNA expression (Fig. 3) and function (data not shown) of CYP3A4 were negligible in both HIECs and Caco-2 cells. The reason for the lack of CYP3A4 in HIECs may be partly explained by interindividual variations in the expression and activity of CYP3A4. The expression and function levels of CYP3A4 are known to have a large interindividual variation (Paine et al., 1997), which could explain the lack of CYP3A4 expression and activity in the HIECs used in this study, which was isolated from the ileum of a single donor (19-year-old Caucasian female). Alternatively, our culture condition may not have been sufficient for full differentiation to express CYP3A4 and other enzymes; therefore, further optimization could be required.

Transmission electron microscopy analysis showed that differentiated HIECs formed polarized columnar monolayers with mature morphologic features including microvilli, tight junctions, and desmosomes, which were similar to those observed in vivo and in the Caco-2 monolayer (Hidalgo et al., 1989). However, the features observed in this study were different from previous morphologic findings (Suzuki et al., 2010) in which flat-shaped cells were noted in differentiated HIECs. Although the cause for this discrepancy was not clear, the fibrillar collagen coating used in this study could accelerate maturation of the HIEC monolayer because this coating is known to accelerate the development of the Caco-2 monolayer (Swiderek and Mannuzza, 1997).

Continuously maintained ISCs conferred the long-term proliferation ability and differentiation capacity of enterocytes to HIECs over 25 passages (Fig. 2). The mRNA of LGR5, an ISC marker, was detected at similar levels during the 8-day cultivation period, whereas the mRNA of IFABP and SI, both enterocyte markers, increased by >10-fold. These results were consistent with the hypothesis that the ISC undergoes asymmetric division to one intestinal stem cell and one progenitor cell, and consequently, the population of ISCs is maintained to constantly generate progenitor cells that can proliferate and differentiate into mature enterocytes over a long period of time (Barker and Clevers, 2010).

The formation of intestinal organoids consisting of enterocytes, goblet cells, enteroendocrine cells, and Paneth cells from human induced pluripotent stem (iPS) cells via ISC was previously demonstrated (Spence et al., 2011); however, the functional characteristics of drug-metabolizing enzymes and transporters were not explored. Iwao et al., (2014) recently demonstrated that enterocyte-like cells that differentiated from human iPS cells via ISCs expressed the mRNAs of peptide transporter 1, also known as solute carrier family 15 member 1, and CYP3A4. These differentiated cells from iPS cells are expected to have similar gene expression levels for drug-metabolizing enzymes and transporters to the human small intestine. In addition, differentiated iPS cells retain the genetic background of the donors; thus, they may facilitate studies on interindividual differences in drug absorption and metabolism. Therefore, advances in the development of in vitro assay systems with HIECs and enterocyte-like cells differentiated from human iPS cells will mutually improve the prediction and elucidation for intestinal function, transport, and metabolism involved in the absorption process in humans.

In conclusion, we established conditions for the long-term culture of adult ISCs with differentiation capability into enterocytes. To the best of

our knowledge, this is the first study to describe the application of a HIEC monolayer to the permeability assay for diverse compounds that are known to be absorbed paracellularly or transcellularly, and/or transported by P-gp, BCRP, and nucleoside transporters. The HIEC monolayer had similarly loose tight junctions to the human small intestine and the distinct mRNA expression of CNT3, which was absent in Caco-2 cells. This study demonstrated that the HIEC monolayer can serve as a novel and superior alternative to the conventional Caco-2 monolayer for predicting oral absorption in humans.

Authorship Contributions

Participated in research design: Takenaka, Harada, Kuze, Chiba, Iwao, Matsunaga.

Conducted experiments: Takenaka, Harada.

Performed data analysis: Takenaka, Harada.

Wrote or contributed to the writing of the manuscript: Takenaka, Harada, Kuze, Chiba, Iwao, Matsunaga.

References

Aldhous MC, Shmakov AN, Bode J, and Ghosh S (2001) Characterization of conditions for the primary culture of human small intestinal epithelial cells. *Clin Exp Immunol* **125**:32–40.

Amidon GL, Sinko PJ, and Fleisher D (1988) Estimating human oral fraction dose absorbed: a correlation using rat intestinal membrane permeability for passive and carrier-mediated compounds. *Pharm Res* **5**:651–654.

Barker N and Clevers H (2010) Leucine-rich repeat-containing G-protein-coupled receptors as markers of adult stem cells. *Gastroenterology* **138**:1681–1696.

Bourgine J, Billaut-Laden I, Happillon M, Lo-Guidice JM, Maunoury V, Imbenotte M, and Broly F (2012) Gene expression profiling of systems involved in the metabolism and the disposition of xenobiotics: comparison between human intestinal biopsy samples and colon cell lines. *Drug Metab Dispos* **40**:694–705.

Chougule P, Herlenius G, Hernandez NM, Patil PB, Xu B, and Sumitran-Holgersson S (2012) Isolation and characterization of human primary enterocytes from small intestine using a novel method. *Scand J Gastroenterol* **47**:1334–1343.

Dixit NM and Perelson AS (2006) The metabolism, pharmacokinetics and mechanisms of antiviral activity of ribavirin against hepatitis C virus. *Cell Mol Life Sci* **63**:832–842.

Endres CJ, Moss AM, Govindarajan R, Choi DS, and Unadkat JD (2009) The role of nucleoside transporters in the erythrocyte disposition and oral absorption of ribavirin in the wild-type and equilibrative nucleoside transporter 1-/- mice. *J Pharmacol Exp Ther* **331**:287–296.

Grossmann J, Walther K, Artinger M, Kiessling S, Steinkamp M, Schmautz WK, Stadler F, Bataille F, Schultz M, and Schölmerich J, et al. (2003) Progress on isolation and short-term ex-vivo culture of highly purified non-apoptotic human intestinal epithelial cells (IEC). *Eur J Cell Biol* **82**:262–270.

Hidalgo IJ, Raub TJ, and Borchardt RT (1989) Characterization of the human colon carcinoma cell line (Caco-2) as a model system for intestinal epithelial permeability. *Gastroenterology* **96**:736–749.

Hu H, Endres CJ, Chang C, Umapathy NS, Lee EW, Fei YJ, Itagaki S, Swaan PW, Ganapathy V, and Unadkat JD (2006) Electrophysiological characterization and modeling of the structure activity relationship of the human concentrative nucleoside transporter 3 (hCNT3). *Mol Pharmacol* **69**:1542–1553.

Irvine JD, Takahashi L, Lockhart K, Cheong J, Tolan JW, Selick HE, and Grove JR (1999) MDCK (Madin-Darby canine kidney) cells: A tool for membrane permeability screening. *J Pharm Sci* **88**:28–33.

Ishida K, Fukao M, Watanabe H, Taguchi M, Miyawaki T, Matsukura H, Uemura O, Zhang Z, Unadkat JD, and Hashimoto Y (2013) Effect of salt intake on bioavailability of mizoribine in healthy Japanese males. *Drug Metab Pharmacokinet* **28**:75–80.

Iwao T, Toyota M, Miyagawa Y, Okita H, Kiyokawa N, Akutsu H, Umezawa A, Nagata K, and Matsunaga T (2014) Differentiation of human induced pluripotent stem cells into functional enterocyte-like cells using a simple method. *Drug Metab Pharmacokinet* **29**:44–51.

Jemnitz K, Veres Z, and Vereczkey L (2002) Coordinate regulation of UDP-glucuronosyltransferase UGT1A6 induction by 3-methylcholanthrene and multidrug resistance protein MRP2 expression by dexamethasone in primary rat hepatocytes. *Biochem Pharmacol* **63**:2137–2144.

Lennernäs H, Nylander S, and Ungell AL (1997) Jejunal permeability: a comparison between the ussing chamber technique and the single-pass perfusion in humans. *Pharm Res* **14**:667–671.

Lennernäs H, Palm K, Fagerholm U, and Artursson P (1996) Comparison between active and passive drug transport in human intestinal epithelial (caco-2) cells in vitro and human jejunum in vivo. *Int J Pharm* **127**:103–107.

Levy E, Ménard D, Delvin E, Montoudis A, Beaulieu JF, Mailhot G, Dubé N, Sinnett D, Seidman E, and Bendayan M (2009) Localization, function and regulation of the two intestinal fatty acid-binding protein types. *Histochem Cell Biol* **132**:351–367.

Lin X, Skolnik S, Chen X, and Wang J (2011) Attenuation of intestinal absorption by major efflux transporters: quantitative tools and strategies using a Caco-2 model. *Drug Metab Dispos* **39**:265–274.

Mangravite LM, Badagnani I, and Giacomini KM (2003) Nucleoside transporters in the disposition and targeting of nucleoside analogs in the kidney. *Eur J Pharmacol* **479**:269–281.

Martínez-Jiménez CP, Castell JV, Gómez-Lechón MJ, and Jover R (2006) Transcriptional activation of CYP2C9, CYP1A1, and CYP1A2 by hepatocyte nuclear factor 4alpha requires coactivators peroxisomal proliferator activated receptor-gamma coactivator 1alpha and steroid receptor coactivator 1. *Mol Pharmacol* **70**:1681–1692.

Matsson P, Bergström CA, Nagahara N, Tavelin S, Norinder U, and Artursson P (2005) Exploring the role of different drug transport routes in permeability screening. *J Med Chem* **48**:604–613.

Matsson P, Pedersen JM, Norinder U, Bergström CA, and Artursson P (2009) Identification of novel specific and general inhibitors of the three major human ATP-binding cassette transporters P-gp, BCRP and MRP2 among registered drugs. *Pharm Res* **26**:1816–1831.

Meier Y, Eloranta JJ, Darimont J, Ismair MG, Hiller C, Fried M, Kullak-Ublick GA, and Vavricka SR (2007) Regional distribution of solute carrier mRNA expression along the human intestinal tract. *Drug Metab Dispos* **35**:590–594.

Ohtsuki S, Schaefer O, Kawakami H, Inoue T, Liehner S, Saito A, Ishiguro N, Kishimoto W, Ludwig-Schwellinger E, and Ebner T, et al. (2012) Simultaneous absolute protein quantification of transporters, cytochromes P450, and UDP-glucuronosyltransferases as a novel approach for the characterization of individual human liver: comparison with mRNA levels and activities. *Drug Metab Dispos* **40**:83–92.

Okayama T, Yoshisue K, Kuwata K, Komuro M, Ohta S, and Nagayama S (2012) Involvement of concentrative nucleoside transporter 1 in intestinal absorption of trifluorothymidine, a novel antitumor nucleoside, in rats. *J Pharmacol Exp Ther* **340**:457–462.

Paine MF, Khalighi M, Fisher JM, Shen DD, Kunze KL, Marsh CL, Perkins JD, and Thummel KE (1997) Characterization of interintestinal and intraintestinal variations in human CYP3A-dependent metabolism. *J Pharmacol Exp Ther* **283**:1552–1562.

Pauli-Magnus C, von Richter O, Burk O, Ziegler A, Mettang T, Eichelbaum M, and Fromm MF (2000) Characterization of the major metabolites of verapamil as substrates and inhibitors of P-glycoprotein. *J Pharmacol Exp Ther* **293**:376–382.

Perreault N and Beaulieu JF (1998) Primary cultures of fully differentiated and pure human intestinal epithelial cells. *Exp Cell Res* **245**:34–42.

Rodgers T and Rowland M (2006) Physiologically based pharmacokinetic modelling 2: predicting the tissue distribution of acids, very weak bases, neutrals and zwitterions. *J Pharm Sci* **95**:1238–1257.

Rosing H, Doyle E, Davies BE, and Beijnen JH (1995) High-performance liquid chromatographic determination of the novel antitumour drug topotecan and topotecan as the total of the lactone plus carboxylate forms, in human plasma. *J Chromatogr B Biomed Appl* **668**:107–115.

Rozehnal V, Nakai D, Hoepner U, Fischer T, Kamiyama E, Takahashi M, Yasuda S, and Mueller J (2012) Human small intestinal and colonic tissue mounted in the Ussing chamber as a tool for characterizing the intestinal absorption of drugs. *Eur J Pharm Sci* **46**:367–373.

Saitoh R, Sugano K, Takata N, Tachibana T, Higashida A, Nabuchi Y, and Aso Y (2004) Correction of permeability with pore radius of tight junctions in Caco-2 monolayers improves the prediction of the dose fraction of hydrophilic drugs absorbed by humans. *Pharm Res* **21**:749–755.

Schmiedlin-Ren P, Thummel KE, Fisher JM, Paine MF, Lown KS, and Watkins PB (1997) Expression of enzymatically active CYP3A4 by Caco-2 cells grown on extracellular matrix-coated permeable supports in the presence of 1alpha,25-dihydroxyvitamin D3. *Mol Pharmacol* **51**:741–754.

Sjöberg Å, Lutz M, Tannergren C, Wingolf C, Borde A, and Ungell AL (2013) Comprehensive study on regional human intestinal permeability and prediction of fraction absorbed of drugs using the Ussing chamber technique. *Eur J Pharm Sci* **48**:166–180.

Skolnik S, Lin X, Wang J, Chen XH, He T, and Zhang B (2010) Towards prediction of in vivo intestinal absorption using a 96-well Caco-2 assay. *J Pharm Sci* **99**:3246–3265.

Spence JR, Mayhew CN, Rankin SA, Kuhar MF, Vallance JE, Tolle K, Hoskins EE, Kalinichenko VV, Wells SI, and Zorn AM, et al. (2011) Directed differentiation of human pluripotent stem cells into intestinal tissue in vitro. *Nature* **470**:105–109.

Sugano K, Takata N, Machida M, Saitoh K, and Terada K (2002) Prediction of passive intestinal absorption using bio-mimetic artificial membrane permeation assay and the paracellular pathway model. *Int J Pharm* **241**:241–251.

Sun D, Lennernas H, Welage LS, Barnett JL, Landowski CP, Foster D, Fleisher D, Lee KD, and Amidon GL (2002) Comparison of human duodenum and Caco-2 gene expression profiles for 12,000 gene sequences tags and correlation with permeability of 26 drugs. *Pharm Res* **19**:1400–1416.

Suzuki A, Sekiya S, Gunshima E, Fujii S, and Taniguchi H (2010) EGF signaling activates proliferation and blocks apoptosis of mouse and human intestinal stem/progenitor cells in long-term monolayer cell culture. *Lab Invest* **90**:1425–1436.

Swiderek MS and Mannuzza FJ (1997) *Effects of ECM Proteins on Barrier Formation in Caco-2 Cells: Becton Dickinson Technical Bulletin No. 421*, BD Biosciences, Franklin Lakes, NJ

Tavelin S, Milovic V, Ocklind G, Olsson S, and Artursson P (1999) A conditionally immortalized epithelial cell line for studies of intestinal drug transport. *J Pharmacol Exp Ther* **290**:1212–1221.

Tavelin S, Taipalensuu J, Hallböök F, Vellonen KS, Moore V, and Artursson P (2003a) An improved cell culture model based on 2/4/A1 cell monolayers for studies of intestinal drug transport: characterization of transport routes. *Pharm Res* **20**:373–381.

Tavelin S, Taipalensuu J, Söderberg L, Morrison R, Chong S, and Artursson P (2003b) Prediction of the oral absorption of low-permeability drugs using small intestine-like 2/4/A1 cell monolayers. *Pharm Res* **20**:397–405.

Varma MV, Obach RS, Rotter C, Miller HR, Chang G, Steyn SJ, El-Kattan A, and Troutman MD (2010) Physicochemical space for optimum oral bioavailability: contribution of human intestinal absorption and first-pass elimination. *J Med Chem* **53**:1098–1108.

Ward JL and Tse CM (1999) Nucleoside transport in human colonic epithelial cell lines: evidence for two Na+-independent transport systems in T84 and Caco-2 cells. *Biochim Biophys Acta* **1419**:15–22.

Yamamoto T, Kuniki K, Takekuma Y, Hirano T, Iseki K, and Sugawara M (2007) Ribavirin uptake by cultured human choriocarcinoma (BeWo) cells and Xenopus laevis oocytes expressing recombinant plasma membrane human nucleoside transporters. *Eur J Pharmacol* **557**:1–8.

Yamashita S, Furubayashi T, Kataoka M, Sakane T, Sezaki H, and Tokuda H (2000) Optimized conditions for prediction of intestinal drug permeability using Caco-2 cells. *Eur J Pharm Sci* **10**:195–204.

Yeung TM, Chia LA, Kosinski CM, and Kuo CJ (2011) Regulation of self-renewal and differentiation by the intestinal stem cell niche. *Cell Mol Life Sci* **68**:2513–2523.

Young JD, Yao SY, Baldwin JM, Cass CE, and Baldwin SA (2013) The human concentrative and equilibrative nucleoside transporter families, SLC28 and SLC29. *Mol Aspects Med* **34**:529–547.

Zhang J, Visser F, King KM, Baldwin SA, Young JD, and Cass CE (2007) The role of nucleoside transporters in cancer chemotherapy with nucleoside drugs. *Cancer Metastasis Rev* **26**:85–110.

Address correspondence to: Dr. Tamihide Matsunaga, Department of Clinical Pharmacy, Graduate School of Pharmaceutical Sciences, Nagoya City University, 3-1 Tanabe-dori, Mizuho-ku, Nagoya 467-8603, Japan. E-mail: tmatsu@phar.nagoya-cu.ac.jp

OPEN ACCESS Freely available online

PLOS | ONE

Histone Deacetylase Inhibitor Valproic Acid Promotes the Differentiation of Human Induced Pluripotent Stem Cells into Hepatocyte-Like Cells

Yuki Kondo[1], Takahiro Iwao[1,2], Sachimi Yoshihashi[2], Kayo Mimori[2], Ruri Ogihara[2], Kiyoshi Nagata[3], Kouichi Kurose[4], Masayoshi Saito[5], Takuro Niwa[5¤a], Takayoshi Suzuki[6], Naoki Miyata[7¤b], Shigeru Ohmori[8], Katsunori Nakamura[1,2], Tamihide Matsunaga[1,2]*

1 Department of Clinical Pharmacy, Graduate School of Pharmaceutical Sciences, Nagoya City University, Nagoya, Japan, **2** Educational Research Center for Clinical Pharmacy, Faculty of Pharmaceutical Sciences, Nagoya City University, Nagoya, Japan, **3** Department of Environmental and Health Science, Tohoku Pharmaceutical University, Sendai, Japan, **4** Department of Food Science and Technology, Graduate School of Marine Science and Technology, Tokyo University of Marine Science and Technology, Tokyo, Japan, **5** DMPK Research Laboratory, Mitsubishi Tanabe Pharma Corporation, Toda, Japan, **6** Graduate School of Medical Science, Kyoto Prefectural University of Medicine, Kyoto, Japan, **7** Department of Organic and Medicinal Chemistry, Graduate School of Pharmaceutical Sciences, Nagoya City University, Nagoya, Japan, **8** Department of Biochemical Pharmacology and Toxicology, Shinshu University, Matsumoto, Japan

Abstract

In this study, we aimed to elucidate the effects and mechanism of action of valproic acid on hepatic differentiation from human induced pluripotent stem cell-derived hepatic progenitor cells. Human induced pluripotent stem cells were differentiated into endodermal cells in the presence of activin A and then into hepatic progenitor cells using dimethyl sulfoxide. Hepatic progenitor cells were matured in the presence of hepatocyte growth factor, oncostatin M, and dexamethasone with valproic acid that was added during the maturation process. After 25 days of differentiation, cells expressed hepatic marker genes and drug-metabolizing enzymes and exhibited drug-metabolizing enzyme activities. These expression levels and activities were increased by treatment with valproic acid, the timing and duration of which were important parameters to promote differentiation from human induced pluripotent stem cell-derived hepatic progenitor cells into hepatocytes. Valproic acid inhibited histone deacetylase activity during differentiation of human induced pluripotent stem cells, and other histone deacetylase inhibitors also enhanced differentiation into hepatocytes. In conclusion, histone deacetylase inhibitors such as valproic acid can be used to promote hepatic differentiation from human induced pluripotent stem cell-derived hepatic progenitor cells.

Citation: Kondo Y, Iwao T, Yoshihashi S, Mimori K, Ogihara R, et al. (2014) Histone Deacetylase Inhibitor Valproic Acid Promotes the Differentiation of Human Induced Pluripotent Stem Cells into Hepatocyte-Like Cells. PLoS ONE 9(8): e104010. doi:10.1371/journal.pone.0104010

Editor: Rajasingh Johnson, University of Kansas Medical Center, United States of America

Received February 14, 2014; **Accepted** July 6, 2014; **Published** August 1, 2014

Funding: This work was supported, in part, by Grants-in-Aid from the Japan Society for the Promotion of Science (23390036, 22390028 and 25460193), by Research on Publicly Essential Drugs and Medical Devices from Japan Health Sciences Foundation (KHB1011 and KHB1208), and by a National Grant-in-Aid from Japanese Ministry of Health, Labor, and Welfare (H22-003). Mitsubishi Tanabe Pharma Corporation provided support in the form of salaries for authors MS & TN, but did not have any additional role in the study design, data collection and analysis, decision to publish, or preparation of the manuscript. The specific roles of these authors are articulated in the 'author contributions' section.

Competing Interests: MS & TN are employees of Mitsubishi Tanabe Pharma Corporation. There are no patents, products in development or marketed products to declare. This does not alter the authors' adherence to all the PLOS ONE policies on sharing data and materials.

* Email: tmatsu@phar.nagoya-cu.ac.jp

¤a Current address: Research & Development Department, Japan Bioindustry Association, Tokyo, Japan
¤b Current address: Institute of Drug Discovery Sciences, Nagoya City University, Nagoya, Japan

Introduction

Induced pluripotent stem (iPS) cells, originally generated from human fibroblasts, are pluripotent and have infinite proliferative potential *in vitro* [1]. Human iPS (hiPS) cells are expected to have various applications, including for studying hepatic drug metabolism and toxicity [2]. Furthermore, hiPS cell-derived hepatocytes may constitute a source of cells for transplantation in the case of a severe liver disease. Previous studies reported hepatic differentiation from hiPS cells using many cytokines such as recombinant growth factors [3–6]. However, cytokines require careful handling because of their structural instability; moreover, they have insufficient hepatic-differentiation activities. In contrast, hepatic differentiation methods that use a combination of cytokines and overexpression of transcriptional factors by viral vectors or co-culture with other cells have been reported [7–10]. Although these methods enhance hepatic functions in differentiated cells, they require considerable technical skills and specialized materials such as modified adenoviruses. Large-scale production of hiPS cell-derived hepatocytes is needed for drug development studies and cell transplantation. However, it is difficult to prepare the reagents required for differentiation of these cells in sufficient quantities using the methods reported previously, and product validation is required.

In general, small-molecule compounds can be synthesized with a high quantity, stability, and purity, and can be used with low risk and lot-to-lot variations; they will thus be highly useful for differentiation into hepatocytes from hiPS cells as differentiation-

inducing-factors. Several studies have reported the use of small-molecule compounds in hepatic differentiation from embryonic stem (ES)/iPS cells [11–13]. However, simple and inexpensive methods for highly efficient hepatic differentiation from hiPS cells have not been established.

Valproic acid (VPA) is a branched short-chain fatty acid that is widely used as an antiepileptic, antimanic, and antimigraine prophylactic drug. The drug raises γ-aminobutyric acid (GABA) concentrations in the human brain by inhibiting GABA transaminase, which participates in GABA degradation, thereby controlling epilepsy [14]. VPA is also known as a potent histone deacetylase (HDAC) inhibitor that is currently being evaluated for cancer treatment [15]. In previous stem cell studies, VPA enabled efficient induction of pluripotent stem cells without introduction of the c-Myc oncogene [16].

Hay *et al.* studied the early stages of hepatic differentiation of human ES cells using sodium butyrate (NaB) [17], which is an HDAC inhibitor [18]. VPA was also used to promote hepatic differentiation from human bone marrow stromal stem cells [19] and mouse ES cells [20]. In both studies, differentiation was initiated by treating undifferentiated cells with VPA, instead of activin A, which is commonly used to differentiate ES/iPS cells into endodermal cells. Although these compounds were used in the initial differentiation processes of undifferentiated cells, the effects of VPA on the maturation processes during differentiation from hiPS cells into hepatocytes remain unknown. Moreover, HDAC inhibitors other than VPA or NaB have not been examined. The present study tested the potential of VPA as a small-molecule compound for hepatic differentiation from hiPS cells. The effect of VPA was evaluated using a multidisciplinary approach that included the assessment of hepatic marker gene expression and enzyme activity, as well as an immunofluorescence assay. The mechanism underlying the VPA-mediated effects was identified using selective inhibitors of HDAC, GABA transaminase, and ion channels, and it was confirmed by functional assays.

Materials and Methods

Materials

The hiPS cell lines Windy [21], Dotcom [7], and Fetch [6], derived from the human embryonic lung fibroblast cell line MRC-5, were provided by Umezawa *et al.* of the National Center for Child Health and Development. Cryopreserved human primary hepatocytes (HPHs; lot. HPCH10/0910463; 10 donors aged 32–76 years) were obtained from XenoTech (Lenexa, KS). Activin A and the hepatocyte growth factor were purchased from PeproTech Inc. (Rocky Hill, NJ). Fetal bovine serum was purchased from Biowest (Nuaillé, France). Accutase was purchased from MS TechnoSystems (Osaka, Japan). Minimal essential medium non-essential amino acids, oncostatin M, dexamethasone, Y-27632, rifampicin (RIF), VPA, gabaculine, trichostatin A (TSA), NaB, vorinostat, procainamide, lidocaine, zonisamide, nifedipine, and midazolam were purchased from Wako Pure Chemical Industries (Osaka, Japan). BD Matrigel matrix Growth Factor Reduced, bupropion, hydroxybupropion, 4′-hydroxydiclofenac-$^{13}C_6$, and hydroxybupropion-d_6 were purchased from BD Biosciences (Bedford, MA). Dimethyl sulfoxide, 2-mercaptoethanol, vigabatrin, ethosuximide, MS-275, acetaminophen, 7-hydroxycoumarin glucuronide, 7-hydroxycoumarin sulfate, and caffeine were purchased from Sigma-Aldrich Co. (St. Louis, MO). (±)-Bufuralol hydrochloride, 1′-hydroxymidazolam, acetaminophen-d_4, 4′-hydroxymephenytoin-d_3, and 1′-hydroxybufuralol-d_9 were purchased from Toronto Research Chemicals (North York, ON, Canada). Diclofenac was purchased from Ultrafine (Manchester, UK). (*S*)-Mephenytoin was purchased from Enzo Life Sciences (Farmingdale, NY). Phenacetin and 7-hydroxycoumarin were purchased from Nacalai Tesque (Kyoto, Japan). 4′-Hydroxymephenytoin, 1′-hydroxybufuralol, and 4′-hydroxydiclofenac were purchased from Sumika Chemical Analysis Service, Ltd. (Tokyo, Japan). 1′-Hydroxymidazolam-d_4 was purchased from Cerilliant Corporation (Round Rock, TX). The mouse monoclonal antihuman albumin (ALB) antibody was purchased from Abcam (Cambridge, UK). KnockOut Serum Replacement (KSR), KnockOut Dulbecco's modified Eagle medium, Roswell Park Memorial Institute (RPMI) + GlutaMax medium, GlutaMax, and Alexa Fluor 568 goat antimouse IgG were purchased from Invitrogen Life Technologies Co. (Carlsbad, CA). Cosmedium 004 (Cosmedium) was purchased from COSMO BIO Co. (Tokyo, Japan). T247 and NCC149 were synthesized as reported previously [22,23]. All other reagents were of the highest quality available.

Differentiation of hiPS cells into hepatocytes

Undifferentiated hiPS cells were cultured as reported previously [6]. The hiPS cells were differentiated into endodermal cells by culturing in RPMI + GlutaMax medium containing 0.5% fetal bovine serum and 100 ng/mL of activin A for 3 days, followed by culturing in RPMI + GlutaMax medium containing 2% KSR and 100 ng/mL of activin A for 2 days. After induction of differentiation, the endodermal cells were dissociated using Accutase for 5 min at 37°C and passaged onto 24- or 96-well plates coated with a thin layer of BD Matrigel matrix Growth Factor Reduced. Y-27632 was added to the culture medium for 24 h after passage at a final concentration of 10 μM. The endodermal cells were differentiated into hepatic progenitor cells (HPCs) by culturing in KnockOut Dulbecco's modified Eagle medium containing 20% KSR, 1% GlutaMax, 1% minimal essential medium nonessential amino acids, 0.1-mM 2-mercaptoethanol, and 1% dimethyl sulfoxide for 7 days. HPCs were then matured by culturing in Cosmedium containing 10 ng/mL of hepatocyte growth factor, 20 ng/mL of oncostatin M, and 100-nM dexamethasone for 10 days. Finally, the cells were cultured in Cosmedium for 3 days. VPA was added to the culture medium for 72 h from day 18 (72-h VPA treatment), for 168 h from day 12 (168-h VPA treatment), or for 312 h from day 12 (312-h VPA treatment) at a final concentration of 2 mM (Fig. 1). Other compounds (1-μM TSA, 5-mM NaB, 5-μM vorinostat, 1.2-μM T247, 1-μM MS-275, 1-μM NCC149, 100-μM gabaculine, 100-μM vigabatrin, 25-μM procainamide, 1-mM lidocaine, 500-μM ethosuximide, 1-μM nifedipine, and 30-μM zonisamide) were added to the culture medium for 168 h from day 12. In the induction study, differentiated cells were treated with 40-μM RIF for the final 48 h of culture.

Cryopreserved human hepatocyte cultures

Cryopreserved HPHs were thawed using a thawing medium without additives (Biopredic, Rennes, France) and seeded on collagen I-coated plates in basal hepatic cell medium (Biopredic) containing additives for hepatocyte seeding medium (Biopredic) for 12 h at 37°C. The medium was then changed to the basal hepatic cell medium containing additives for hepatocyte culture (Biopredic), and the cells were cultured for 36 h.

Real-time RT-PCR analysis

Total RNA was extracted using an RNeasy Mini Kit (QIAGEN, Valencia, CA) and first-strand cDNA was generated using a PrimeScript RT Reagent Kit (Takara Bio Inc., Otsu, Japan), according to the manufacturer's instructions. Real-time

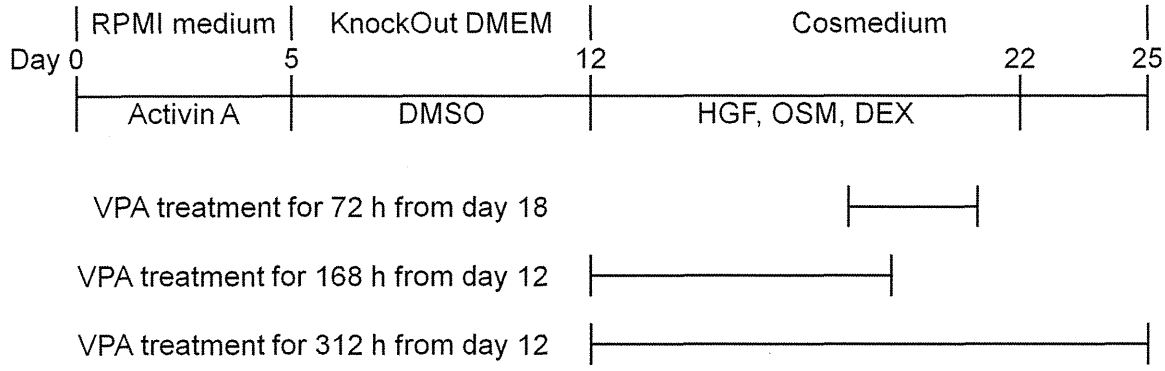

Figure 1. Schematic protocol for hepatic differentiation of hiPS cells. Human iPS (hiPS) cells were differentiated into endodermal cells using Roswell Park Memorial Institute (RPMI) + GlutaMAX medium containing 100 ng/mL of activin A for 5 days, and then into hepatic progenitor cells (HPCs) using KnockOut Dulbecco's modified Eagle medium (KnockOut DMEM) containing 1% dimethyl sulfoxide (DMSO) for 7 days. Thereafter, HPCs were matured using Cosmedium 004 (Cosmedium) containing 10 ng/mL of hepatocyte growth factor (HGF), 20 ng/mL of oncostatin M (OSM), and 100 nM of dexamethasone (DEX) for 10 days. Finally, the cells were cultured in only Cosmedium for 3 days. Valproic acid (VPA) was added to the culture medium for 72 h from day 18, 168 h from day 12, or 312 h from day 12 at a final concentration of 2 mM.
doi:10.1371/journal.pone.0104010.g001

RT-PCR was performed using SYBR Premix EX Taq II (Takara Bio Inc.), and products were detected using an ABI 7300 Real Time PCR System (Applied Biosystems, Carlsbad, CA). The mRNA expression levels were normalized to those of glyceraldehyde-3-phosphate dehydrogenase. The primers used in this experiment are listed in Table 1.

Immunofluorescence staining

Cells were fixed for 20 min at room temperature in 4% paraformaldehyde, and then permeabilized in methanol for 5 min at −30°C. After blocking with 2% skim milk for 30 min at room temperature, cells were incubated with the mouse monoclonal antihuman ALB antibody (dilution, 1:200) for 60 min at room temperature, followed by incubation with a 1:500 dilution of Alexa Fluor 568 goat antimouse IgG for 60 min at room temperature. Finally, cells were incubated with 1 μg/mL of 4′,6-diamidino-2-phenylindole for 5 min at room temperature and observed under an ECLIPSE *Ni* microscope (NIKON Inc., Tokyo, Japan).

Determination of drug-metabolizing enzyme activities

Differentiated hiPS cells were incubated in Cosmedium containing 40-μM phenacetin, 50-μM bupropion, 5-μM diclofenac, 100-μM (*S*)-mephenytoin, 5 μM-bufuralol, 5-μM midazolam, and 10-μM 7-hydroxycoumarin for 6 or 24 h at 37°C. Thereafter, 40-μL aliquots of reaction medium were collected, and the reactions were stopped by adding 40 μL of ice-cold acetonitrile containing stable isotope-labeled internal standards for quantification. The metabolites were measured using ultra performance liquid chromatography–tandem mass spectrometry (UPLC–MS/MS). The probe substrates of drug-metabolizing enzymes and the metabolites used in this experiment are summarized in Table 2.

For UPLC–MS/MS analyses, samples were thawed and centrifuged at 13,000 rpm for 3 min at 4°C. To measure metabolites, 2-μL aliquots of supernatant were injected into the UPLC–MS/MS apparatus. UPLC was performed using a Water ACQUITY UPLC system (Waters Corporation, Milford, MA). UPLC was performed using an Aquity UPLC BEH C18 column (2.1×50 mm, 1.7 μm), mobile phases of water containing 0.025% formic acid, and methanol containing 0.025% formic acid, at a flow rate of 0.8 mL/min, a column temperature of 55°C, and a

Table 1. Sequences of primers for real-time RT-PCR analysis.

Gene names	Forward primer sequences (5′- -3′)	Reverse primer sequences (5′- -3′)
ALB	GAGCTTTTTGAGCAGCTTGG	GGTTCAGGACCACGGATAGA
AFP	AGCTTGGTGGTGGATGAAAC	TCTGCAATGACAGCCTCAAG
TAT	ATCTCTGTTATGGGGCGTTG	TGATGACCACTCGGATGAAA
PXR	AGGATGGCAGTGTCTGGAAC	AGGGAGATCTGGTCCTCGAT
CYP2C9	GACATGAACAACCCTCAGGACTTT	TGCTTGTCGTCTCTGTCCCA
CYP2C19	GAACACCAAGAATCGATGGACA	TCAGCAGGAGAAGGAGAGCATA
CYP3A4	CTGTGTGTTTCCAAGAGAAGTTAC	TGCATCAATTTCCTCCTGCAG
UGT1A1	CAGCAGAGGGGACATGAAAT	ACGCTGCAGGAAAGAATCAT
GAPDH	GAGTCAACGGATTTGGTCGT	GACAAGCTTCCCGTTCTCAG

The abbreviations used are: ALB, albumin; AFP, α-fetoprotein; TAT, tyrosine aminotransferase; PXR, pregnane X receptor; CYP, cytochrome P450; UGT, UDP-glucuronosyltransferase; GAPDH, glyceraldehyde-3-phosphate dehydrogenase.
doi:10.1371/journal.pone.0104010.t001

Table 2. Probe substrates of drug-metabolizing enzyme and the metabolites.

Drug-metabolizing enzyme	Substrate	Metabolite
CYP1A1/2	Phenacetin	Acetaminophen
CYP2B6	Bupuropion	Hydroxybupropion
CYP2C9	Diclofenac	4′-Hydroxydiclofenac
CYP2C19	(*S*)-Mepehnytoin	4′-Hydroxymephenytoin
CYP2D6	Bufuralol	1′-Hydroxybufuralol
CYP3A4/5	Midazolam	1′-Hydroxymidazolam
UGT	7-Hydroxycoumarin	7-Hydroxycoumarin glucuronide
SULT	7-Hydroxycoumarin	7-Hydroxycoumarin sulfate

The abbreviations used are: CYP, cytochrome P450; UGT, UDP-glucuronosyltransferase; SULT, sulfotransferase.
doi:10.1371/journal.pone.0104010.t002

sample temperature of 8°C. Eluents were analyzed in the multiple reaction monitoring mode, under positive and negative electrospray ionization conditions using a Waters Xevo TQ-S mass spectrometer. MS was performed using a capillary voltage of 0.5 kV, a source temperature of 150°C, a desolvation temperature of 650°C, a cone gas flow of 150 L/h, a desolvation gas flow of 1,200 L/h, and a collision gas flow of 0.18 mL/min using argon as the collision gas.

To correct for drug-metabolizing enzyme activities, plated cells were lysed and total protein content was measured using a Pierce BCA protein assay kit (Thermo Fisher Scientific Inc., Waltham, MA), according to the manufacturer's instructions.

Determination of HDAC activity

Cells were incubated in 100 μL of Williams' medium E (without phenol red) with or without 2-mM VPA for 30 min at 37°C. Subsequently, 100 μL of HDAC-Glo I/II Reagent was added to each well, and the cells were incubated for 15 min at room temperature. After incubation, 100 μL of supernatant was transferred to white-walled plates, and the degrees of luminescence for 0.5 sec of integration time were measured using GloMAX-Multi+ (Promega). To correct for HDAC activity, cell numbers were counted using a Cell Counting Kit-8 (DOJINDO, Kumamoto, Japan) before assay of HDAC activity, according to the manufacturer's instructions.

Statistical analysis

Levels of statistical significance were assessed using Student's *t*-test, and multiple comparisons were performed using analysis of variance followed by Dunnett's test. A p value of <0.05 was considered statistically significant.

Results

VPA-induced differentiation from hiPS cells into hepatocytes

To investigate whether VPA promotes differentiation from hiPS cells into hepatocytes, the effects of VPA were examined at several time points. Hepatic differentiation from hiPS cells was evaluated by measuring the expression of ALB, α-fetoprotein (AFP), and tyrosine aminotransferase (TAT), which are hepatocyte-specific marker proteins, and of the pregnane X receptor (PXR), which is a nuclear receptor that regulates cytochrome P450 (CYP) 3A4 expression. Compared with the control group (VPA nontreatment), ALB and PXR mRNAs increased by 7- and 1.7-fold after the 72-h VPA treatment, respectively. These mRNAs also increased by 32- and 5-fold after the 168-h VPA treatment, respectively (Fig. 2A). After the 312-h VPA treatment, the ALB mRNA increased by 8-fold, whereas the PXR mRNA decreased to 0.2-fold. The TAT mRNA expression increased by 1.5- and 4-fold after 72- and 168-h VPA treatments, respectively, but it decreased to 0.3-fold after the 312-h VPA treatment. The AFP mRNA expression was altered by 1.5-, 3.8-, and 1.2-fold after the 72-, 168-h, and 312-h VPA treatments, respectively. HPHs were used to evaluate hepatic differentiation from hiPS cells. In drug-development studies, HPHs are usually tested after cultivation for a few days, whereas it is known that the function of HPHs is reduced dramatically by cultivation after thawing. Therefore, we used HPHs cultured for 48 h (HPHs 48 h) as the positive control. The mRNA expression of ALB in differentiated cells after the 168-h VPA treatment was 42-fold higher than that detected in HPHs 48 h, and the mRNAs of TAT and PXR were expressed at levels that were similar to those of HPHs 48 h. The AFP mRNA in all groups of differentiated cells was higher than that observed in HPHs 48 h.

CYP3A4, a major CYP isoform in the human liver, is also an excellent marker of hepatic differentiation. The mRNA expression of CYP3A4 in the differentiated cells increased by 5.7-, 7.5-, and 3.5-fold after the 72-, 168-, and 312-h VPA treatments, respectively, compared with control group (Fig. 2B). Furthermore, the CYP3A4 mRNA was markedly induced by treatment with RIF in the 72- and 168-h VPA treatment groups. However, the CYP3A4 mRNA expression was unaffected by RIF after the 312-h VPA treatment.

Morphological changes and immunofluorescence staining of ALB

The morphology of hiPS cells changed dramatically during differentiation (Fig. 3). Binuclear cells, which are typical morphology of mature hepatocytes, were increased by the 168-h VPA treatment compared with the control group (Fig. 3C–F). Interestingly, vasculature-like structures in differentiated cells also appeared after the 312-h VPA treatment (data not shown). Most differentiated hiPS cells exhibited anti-ALB antibody during immunofluorescence staining after the 168-h VPA treatment, whereas the staining intensity was low in differentiated cells without the VPA treatment under the same staining conditions (Fig. 4A, B).

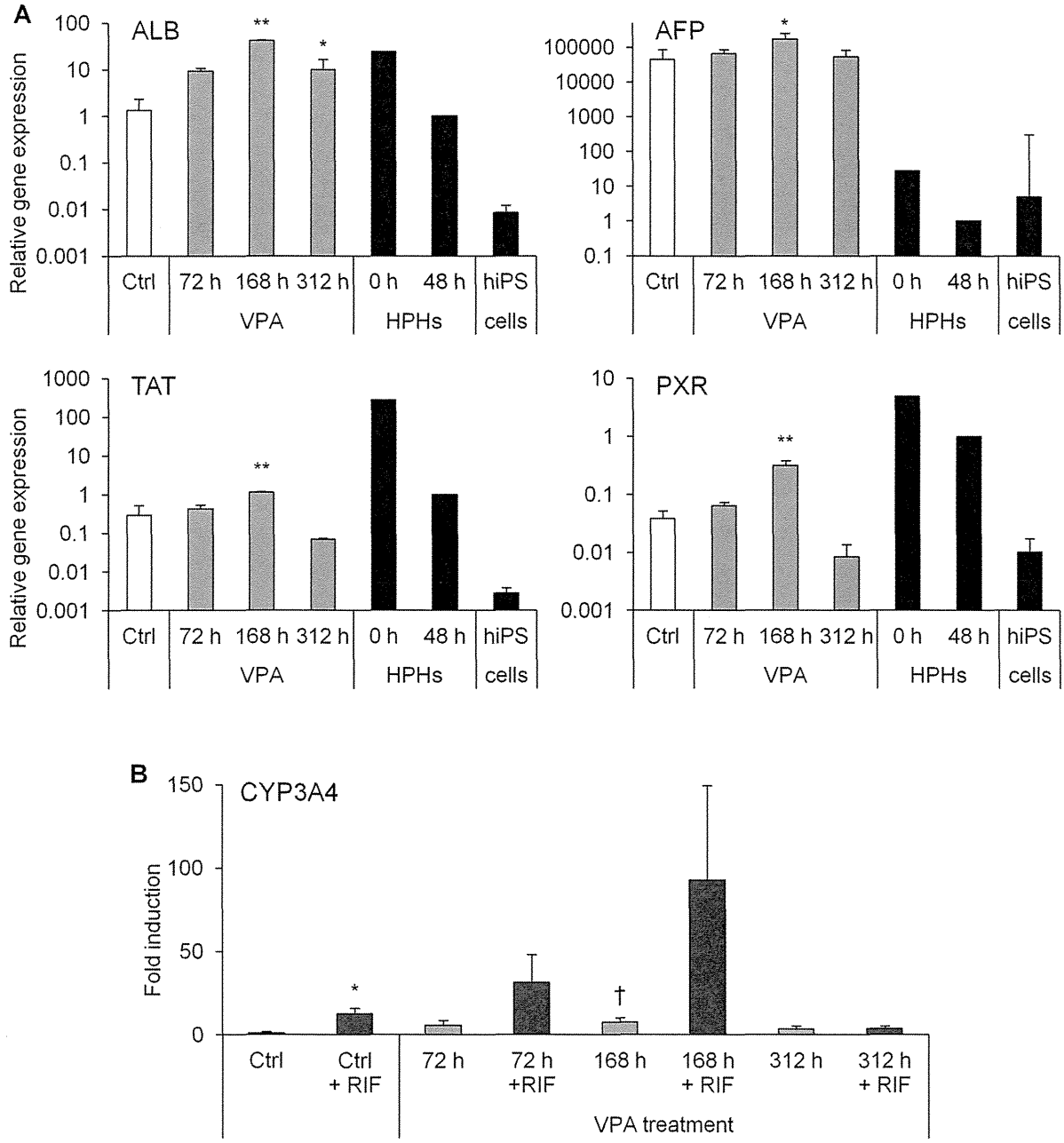

Figure 2. Effects of VPA on hepatic marker gene expression and induction of the CYP3A4 mRNA by RIF. Human iPS (hiPS) cells (Windy) were differentiated into hepatocytes. Valproic acid (VPA) was added to the medium for 72 h from day 18 (72 h), 168 h from day 12 (168 h), or 312 h from day 12 (312 h). (A) Cryopreserved human primary hepatocytes (HPHs) were cultured for 0 (just after thawing) and 48 h. Each bar represents the mean ± standard deviation ($n=3$). The graph represents gene expression relative to that detected in HPHs cultured for 48 h. Levels of statistical significance compared with VPA-untreated hepatocyte-like cells [control (Ctrl)]: *$P<0.05$ and **$P<0.01$; and (B) hiPS cell-derived hepatocyte-like cells were treated with 40-μM rifampicin (RIF) for the last 48 h of culture. Each bar represents the mean ± standard deviation ($n=2$–3). The graph represents gene expression relative to that detected in VPA-untreated hepatocyte-like cells without RIF. Levels of statistical significance compared with Ctrl in the RIF-untreated group (†), and RIF-treated group compared with each RIF-untreated group (*), respectively: †$P<0.05$ and *$P<0.05$. The abbreviations used are: AFP, α-fetoprotein; ALB, albumin; TAT, tyrosine aminotransferase; PXR, pregnane X receptor; CYP, cytochrome P450.
doi:10.1371/journal.pone.0104010.g002